Mesoscale Organization of Springtime Rainstorms in Oklahoma

ROBERT A. HOUZE, JR.

Department of Atmospheric Sciences, University of Washington, Seattle, Washington

BRADLEY F. SMULL

Mesoscale Research Division, National Severe Storms Laboratory, NOAA, Boulder, Colorado

PETER DODGE

Hurricane Research Division, Atlantic Oceanographic and Meteorological Laboratory, NOAA, Miami, Florida

(Manuscript received 23 January 1989, in final form 28 August 1989)

ABSTRACT

Radar reflectivity and raingage data obtained during six springtimes indicate the types of mesoscale organization that occur in association with major rain events in Oklahoma (at least 25 mm of rain in 24 h over an area exceeding 12 500 km^2). In these storms the primary rain area is found to be a contiguous region of precipitation 10s to 100s of km in scale that consists partly of deep convection and partly of stratiform rain. The patterns of rain formed by the convective and stratiform areas comprise a continuous spectrum of mesoscale structures. About two-thirds of the cases examined exhibited variations on the type of organization in which convective cells arranged in a moving line are followed by a region of stratiform rain. Storm organization was graded according to the degree to which it matched an idealized model of this "leading-line/trailing-stratiform" structure. The precipitation pattern was further graded according to whether its structure was relatively symmetric with respect to an axis normal to and passing through the midpoint of the line, or asymmetric, in which case the storm was biased toward having stronger, more discrete convective structure at the upwind (south or southwestern) end of the line and/or the most extensive stratiform precipitation behind the downwind (north to northeastern) end of the line. About one-third of the cases examined displayed much more chaotic, unclassifiable arrangements of convective and stratiform areas.

Among the cases with leading-line/trailing-stratiform structure, severe weather was most frequent in systems with (i) a strong degree of leading-line/trailing-stratiform structure, in which a solid, relatively uniform, arc-shaped line had stratiform rain centered symmetrically behind it, and (ii) a weaker degree of leading-line/trailing-stratiform structure in which a southwest–northeast line was biased toward having narrow, intensely convective, irregularly spaced cell structure at its southwestern (upwind) end and stratiform rain confined to the region behind the broader northeastern (downwind) portion of the line. Although all mesoscale organization types were characterized by all types of severe weather, the type (ii) cases were the most prolific category in terms of tornado and hail production, while type (i) cases were prone to be associated with flooding. The chaotic, unclassifiable cases, which exhibited no line organization, had just as much severe weather as the cases with line organization, but were more likely to produce hail and somewhat less likely to produce tornadoes and flooding than the systems with line structure.

Major rain events occurred whenever a mesoscale convective complex (MCC) was passing over the study area, unless the MCC was dissipating or merely skirting the area. However, 75% of the major rain events occurred under cloud shields that failed to meet the MCC criteria explicitly, although they often resembled MCCs qualitatively. No particular type of mesoscale radar-echo organization was favored when cloud shields meeting the MCC criteria were observed. A slight preference for the more chaotic type of organization was suggested; however, the data sample is not large enough for this finding to be regarded as conclusive.

Mean soundings and hodographs generally show no sign of a low-level jet in environments associated with chaotically arranged rain areas that lacked any line structure. On the other hand, a low-level jet and resulting curved hodograph were typically associated with cases in which line organization was evident. The wind shear in the low-to-mid troposphere, the bulk Richardson number and other familiar parameters characterizing squall line environments are consistent with results from recent modeling studies. When leading-line/trailing-stratiform structure was present, the cross-line shear in the environment was of a magnitude associated with model simulations in which a rearward sloping updraft circulation favorable to trailing-stratiform anvil formation quickly develops. The along-line component of shear was greater when the squall system structure was of the asymmetric type and the degree of leading-line/trailing-stratiform structure was not as strong, i.e. in those mesoscale systems favoring tornado occurrence.

1. Introduction

Springtime precipitation over the central United States is associated primarily with thunderstorms.

Corresponding author address: Professor R. A. Houze, Department of Atmospheric Sciences, AK-40, University of Washington, Seattle, Washington 98195.

These storms not only bring beneficial rainfall but also the threat of severe weather. In the past, considerable scientific attention has been given to the individual cumulonimbus elements in which large hail, tornadoes, and local heavy downpours of rain tend to develop. The individual cumulonimbus elements have characteristic horizontal dimensions in the range 5–50 km. However, even the most casual inspection of radar screens during major warm season rainstorms reveals that the main areas of precipitation are typically 100–500 km in horizontal dimension—much larger than cumulus scale. Intense cumulonimbus cells are located within these mesoscale rain areas. But in addition to convective cells, which are often arranged in lines, the mesoscale rain areas contain broad areas of lighter stratiform precipitation connected with the groups or lines of cells. These mesoscale complexes of convective and stratiform precipitation develop wide upper-level cloud shields (typically 500 km or more in horizontal dimension) delineated by contours of low temperature in infrared satellite imagery. The widest and coldest of these cloud shields identify the "mesoscale convective complexes" described by Maddox (1980).

A number of midlatitude mesoscale convective precipitation systems have been studied in detail. In some of these cases, the convective cells occur in an advancing line trailed by a 50–100 km wide region of stratiform rain (e.g., Newton 1950; Fujita 1955; Pedgley 1962; Ogura and Liou 1980; Smull and Houze 1985, 1987a, 1987b; Srivastava et al. 1986; Leary and Rappaport 1987; Kessinger et al. 1987; Rutledge et al. 1988). These cases resemble tropical squall lines (e.g., Zipser 1969, 1977; Houze 1977; Fortune 1980; Gamache and Houze 1982, 1983, 1985; Houze and Rappaport 1984; Roux et al. 1984). In other midlatitude storms, intense cells develop systematically on the south to southwestern end of a convective line, while dissipating cells and stratiform cloud and rain are found toward its north to northeastern end (e.g., Newton and Fankhauser 1964; Houze et al. 1989).

From these case studies, it would appear that there are at least two recognizable modes of organization of precipitation within midlatitude mesoscale convective systems: convective lines with trailing-stratiform rain areas, and convective lines with intense convection on their southern ends and weak convection and stratiform rain toward their northern ends. But how representative are these few examples of all warm season midlatitude rainstorms? Day-to-day examination of radar echo patterns in these storms reveals an at times bewildering variety of mesoscale spatial arrangements of convective and stratiform echoes. In this study, we have sought to identify systematically the various modes of organization of radar echo patterns that occurred in springtime rainstorms in central Oklahoma over a six-year period. The objective of this effort is to establish a background climatology of mesoscale rainfall organization against which the representativeness of any individual warm-season midlatitude rainstorm can be judged.

Springtime in central Oklahoma was chosen as the focus of the study since it is the wettest season in that region, with over 40% of the average annual precipitation falling in a three-month period, and because a rich source of data describing storms in that area was available. From 1964 through the mid-1980s, the National Severe Storms Laboratory (NSSL) in Norman, Oklahoma, annually conducted a Spring Program in which data were collected to support the laboratory's research. As part of this effort, the NSSL WSR-57 radar was operated routinely, and 35-mm microfilm photographs were taken of the scope whenever the radar was operating. The display was usually set to show echoes out to a maximum range of about 200 km, providing more detail than the setting of approximately 450 km typically used for scope photography at National Weather Service radars. The archive of Spring Program radar microfilms at NSSL was thus a suitable and readily available resource allowing a thorough survey of warm season midlatitude mesoscale precipitation systems, especially those that occur over the Great Plains of the United States.

The NSSL microfilm data have also been used by Bluestein and Jain (1985) and Bluestein et al. (1987) in a survey of Oklahoma squall lines. Their studies differ from ours in that they focused strictly on storms that exhibited lines of cumulonimbus and sought insight into factors determining the formation of such lines (regardless of how much rain fell). Our study concentrates not just on lines but on all storm organization types that are associated with significant rainfall over central Oklahoma. These major rain episodes are important both because they are the primary source of water for agriculture and other practical purposes and because they represent the situations in which the largest amounts of latent heat are released into the atmosphere. Some storms both produce large areal rainfall and exhibit lines and thus appear both in our data sample and those of Bluestein and collaborators. Where overlap in the data samples occurs, we find ourselves in reasonable agreement with their classifications of line structure. Our objective, however, remains distinct from theirs. We seek to identify and characterize recurrent patterns within the entire spectrum of mesoscale organization that occurs in major springtime rainstorms. Convective lines are but a part of this spectrum.

2. Data

a. Period of the study

Data were obtained for April, May, and June of 1977–82, encompassing six consecutive NSSL Spring Programs. All of the major precipitation events that occurred in central Oklahoma during these months

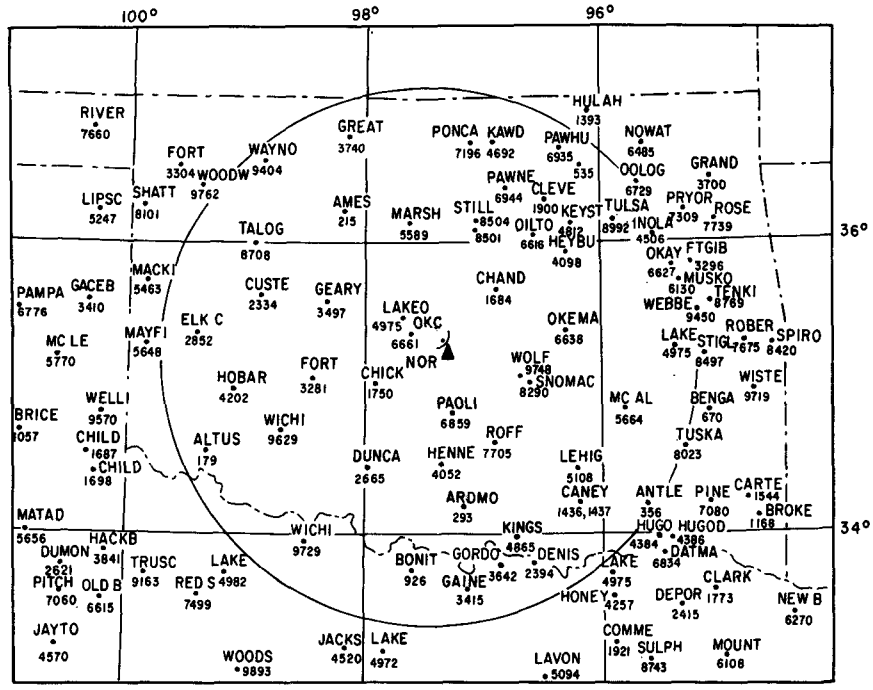

FIG. 1. Map of geographical area considered in the study showing Oklahoma and adjacent states (dash-dot lines denote state boundaries). Hourly Precipitation Data raingage locations are marked by dots and identified by first five letters of station name and identification code. Circle outlines the "Study Area" and corresponds to 200 km range from the NSSL WSR-57 radar located at Norman, Oklahoma (NOR).

have been examined. Six types of data were referred to, and these are described in the following subsections.

b. Radar data

The primary data for this study were microfilms of the display of the NSSL WSR-57 radar, a 10-cm wavelength system with a peak power of 305 kW and a beamwidth of 2.2°. This radar was normally operated in a surveillance mode, with an elevation angle of 0.8° and a maximum range of 240 km displayed on the Plan-Position Indicator (PPI). The 200-km radius area covered by the radar is shown in Fig. 1, and is referred to hereafter as the *study area.* Reflectivity was displayed as a set of contours, referred to as levels 1–6, in order of increasing intensity. Visual analysis of the radar echoes was relatively straightforward. Even though the intensity-level settings changed slightly from year to year (Table 1), levels 4 and above always indicated convection (with the exception of ground clutter). Particular attention was given to the occurrence of *mesoscale precipitation systems,* which for the purposes of this study we defined to be a distinct group of echoes or contiguous area of radar echo that extended spatially over horizontal distances ~ 100 km or more and exhibited time continuity over several hours. The particular structure of these systems is the subject of later sections.

TABLE 1. Reflectivity values (dBZ) corresponding to intensity contours on microfilmed PPI displays from WSR-57 radars used in study.

Radar	Year	From (Month/day)	To	Contour levels 1	2	3	4	5	6	7
NSSL	1977	1/1	5/2	16	21	29	38	48	57	
NSSL	1977	5/3	5/15	16	21	32	43	54	65	
NSSL	1977	5/16	5/19	20	24	34	46	58	70	
NSSL	1977	5/20	12/31	20	26	35	46	57	67	
NSSL	1978	1/1	4/9	—	20	30	40	50	60	70
NSSL	1978	4/10	12/31	20	30	40	45	50	60	
NSSL	1979–82	1/1	12/31	20	25	35	45	55	65	
OKC	1977–82	1/1	12/31	*	30	41	46	50	57	

* Level 1 for the OKC radar comprised all echo > 1/2 dBZ above the minimum detectable signal and <30 dBZ.

The NSSL WSR-57 radar was not always operated to collect data 24 h a day. The radar was often shut down around midnight, even if a major mesoscale system filled the screen. The resulting data gaps were filled in with films from the Oklahoma City National Weather Service WSR-57 radar, located 22 km northwest of the NSSL radar. Although the Oklahoma City radar operated continuously, films of its display were of limited quality and occasionally so poor that interpretation of the data was limited to the determination of the existence or non-existence of echo.

c. Hourly precipitation data

To determine when major precipitation events occurred in the study area, we obtained hourly precipitation data for Oklahoma and Texas on magnetic tapes from the National Climatic Data Center. Locations of stations are shown in Fig. 1. The data were edited to remove points where "no precipitation" had been recorded instead of "missing data." The edited hourly data were summed to obtain daily amounts at each station. Since mesoscale cloud systems over Oklahoma in the spring often continue well past local midnight and dissipate in the early morning, the daily precipitation amounts were computed on a local noon-to-noon basis (1800 to 1800 UTC) to capture distinct events most effectively.

We used the daily rainfall amounts computed from the edited hourly precipitation data for April, May, and June 1977–1982, to select the storms included in this study. Our intent was to consider only those systems that produced significant rainfall over a large portion of Oklahoma. Accordingly, a *major rain event* was defined as a 24-h period in which 25 mm or more of rain fell over 10% or more of the study area designated by the circle in Fig. 1.

To identify major rain events, the edited noon-to-noon rain amounts were gridded and contoured objectively. On the resulting maps (e.g., Fig. 2), the fraction of the study area covered by $\geq$25 mm of rain was measured. The ratio of that area to the total study area (125 000 km^2) was computed. Cases with $\geq$10% coverage were then defined to be the major rain events and included in the study. A total of 55 major rain events (an average of $\approx$9 per year) were identified (Table 2). Considerable variability in the annual number of rain events was noted, however, ranging from six in 1977 to a maximum of 13 in 1980. The frequency distribution of these events (summed over the 1977–82 study period) viewed in 10-day intervals throughout the April–June period (Fig. 3) shows that they were most prone to occur during the months of May and June, with a prominent peak during late May. Examination of the climatology of several raingage stations indicates that the $\approx$9 major rain events occurring during a typical spring account for about 25% of the annual precipitation in central Oklahoma (Dodge 1985).

d. Severe weather reports

To examine the association of severe weather occurrence with mesoscale radar echo patterns, we referred to the monthly U.S. government publication *Storm Data,* in which reported severe weather events are arranged for each state chronologically and by county. These reports are included on the basis of chance observation by the public and/or spotters, reported crop or property damage, injury or loss of life, etc., and are not strictly related to criteria set forth for, say, severe thunderstorms. For example, a hailstorm might be listed if widespread crop damage occurred even though the largest hail failed to reach 2 cm in diameter. From these data, the occurrence of tornadoes, hailstorms, funnel clouds, lightning, flooding, windstorms, and heavy rain was tabulated.

A total of 971 reports was recorded over the study area for April, May, and June 1977–1982. Reports were first sorted by type and by dividing the April–June calendar into nine 10-day intervals within which reports from the entire five-year study period were considered. We then returned to the raw dataset and prepared daily maps (local midnight-to-midnight) showing all reported severe weather in the study area for these months. Figure 4 is an example of a very active day, 20 May 1977. Each symbol indicates the type and location of an event. The times of the observations are plotted next to the symbols. These symbols were subsequently transferred to radar echo maps corresponding to the time of the severe weather event. In this way, the relationship of severe weather to the structure and evolution of individual mesoscale precipitation systems occurring during major rain events could be studied.

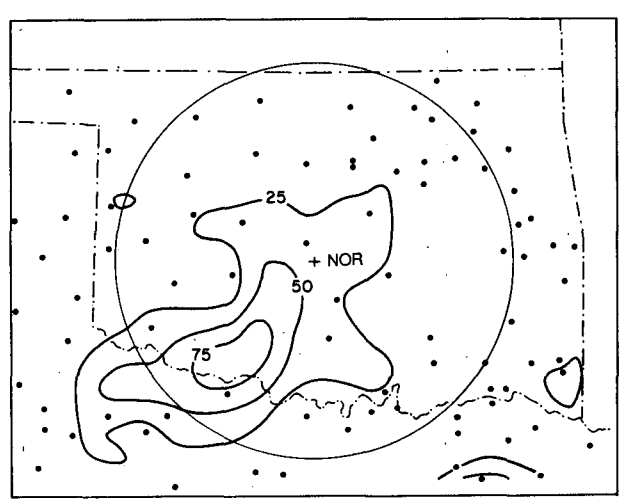

FIG. 2. Accumulated rainfall map (isohyets in mm) for a typical "Major Rain Event" (defined in text) on 2–3 May 1982. Dots correspond to locations of hourly precipitation data stations used to generate objective isohyetal analysis. Circle encloses study area centered on NSSL WSR-57 radar (NOR). Dash-dot lines denote state boundaries.

TABLE 2. Major rain events (see text for definition) in Oklahoma during study period (April–June of 1977–1982). "Date" denotes year/month/day of 24-h period ending at 1800 UTC (noon local time) corresponding to event. "Heavy Rain Coverage" denotes percentage (%) of study area (defined in text) covered by rainfall ≥ 25 mm. "Stratiform Echo Coverage" denotes maximum percentage (%) of study area covered by stratiform radar echo during event. "Time of Maximum Stratiform Echo" is time (UTC) when maximum stratiform echo coverage was observed. An entry of "M" indicates that radar data were incomplete or missing.

Date (year/month/day)	Heavy rain coverage (%)	Stratiform echo coverage (%)	Time of maximum stratiform echo (UTC)
77/4/21	18	21	0635
77/5/02	15	13	1240
77/5/17	29	17	0523
77/5/20	62	23	0400
77/5/21	64	21	0800
77/5/27	25	40	0613
78/4/10	47	25	0327
78/5/03	91	37	0117
78/5/20	13	13	0157
78/5/21	21	38	0943
78/5/27	34	21	1126
78/5/28	78	37	0557
78/6/05	16	23	1142
78/6/06	34	19	1333
78/6/18	17	M	M
78/6/22	27	6	1503
79/4/11	38	22	2154
79/5/03	27	25	1703
79/5/04	26	32	1903
79/5/21	60	41	0648
79/5/22	15	10	1848
79/6/09	79	26	2120
80/4/24	12	16	1700
80/4/25	19	20	1702
80/4/26	43	19	2300
80/5/02	22	18	1438
80/5/15	56	36	1606
80/5/16	46	60	1809
80/5/18	29	17	0750
80/5/27	24	17	1030
80/5/29	35	17	1024
80/5/30	22	8	2339
80/6/17	25	14	1425
80/6/19	11	18	1001
80/6/20	32	23	1237
81/5/09	19	10	0400
81/5/10	31	M	M
81/5/24	10	11	0121
81/5/29	18	28	0632
81/5/30	17	10	0553
81/6/02	33	40	0558
81/6/03	15	13	1102
81/6/15	18	10	1601
81/6/16	25	28	0000
81/6/30	25	M	M
82/5/06	61	43	0312
82/5/12	75	45	1600
82/5/13	44	65	0602
82/5/16	18	16	1600
82/5/17	82	53	0600
82/5/24	29	15	0031
82/5/28	51	29	0452
82/6/04	11	M	M
82/6/16	18	3	0150
82/6/24	22	26	0904

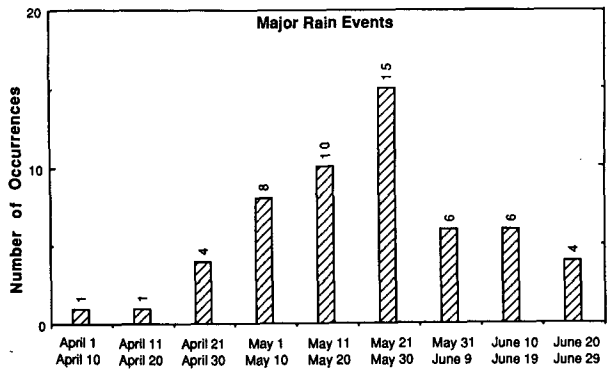

FIG. 3. Histogram showing frequency distribution of Major Rain Events by 10-day intervals throughout April-June for the entire 1977–82 study period.

e. *Satellite data*

Imagery from the GOES-East satellite was obtained for a sector that provided a good view of the study area and surrounding region. Hourly (and occasionally half-hourly) enhanced infrared images depicting blackbody temperature contours at −32, −41, −52, −62 and −80°C (the "Curve MB" enhancement) were examined with attention to the origin, structure, and evolution of cloud patterns accompanying major rain events over Oklahoma. While these data were useful in forming impressions concerning the nature of mesoscale cloud features associated with significant widespread rainfall, gaps in the dataset rendered it less than ideal for comprehensive analysis. A supplementary data source was provided by Dr. E. Tollerud of NOAA's Forecast Systems Laboratory, who has compiled a comprehensive list of those cloud shields qualifying as mesoscale convective complexes (MCCs) according to the definition set forth by Maddox (1980). These systems are noted for their large size, nearly round shape, and substantial duration as seen in infrared satellite imagery. The list is based partially on published summaries of MCC occurrence (e.g., Maddox et al. 1982; Rodgers et al. 1983) and includes the times and locations of the origin (first convective clouds), initiation (when the MCC size/shape criteria were first met), maximum extent (when the cold cloud shield covered the greatest area), and dissipation (after which the size/shape criteria were no longer met) of all MCCs observed during 1978–85. It should be emphasized that some subjectivity is implicit in even the most careful application of Maddox's criteria due to vagaries of the data and the complicated nature of the phenomena.

Satellite data for 49 of the 55 major rain events (i.e., all except those during 1977, for which no satellite data were available) were evaluated. In this manner, those MCCs corresponding to the precipitation areas that contributed to major rain events were noted. On the basis of this information, MCC frequency was tabulated

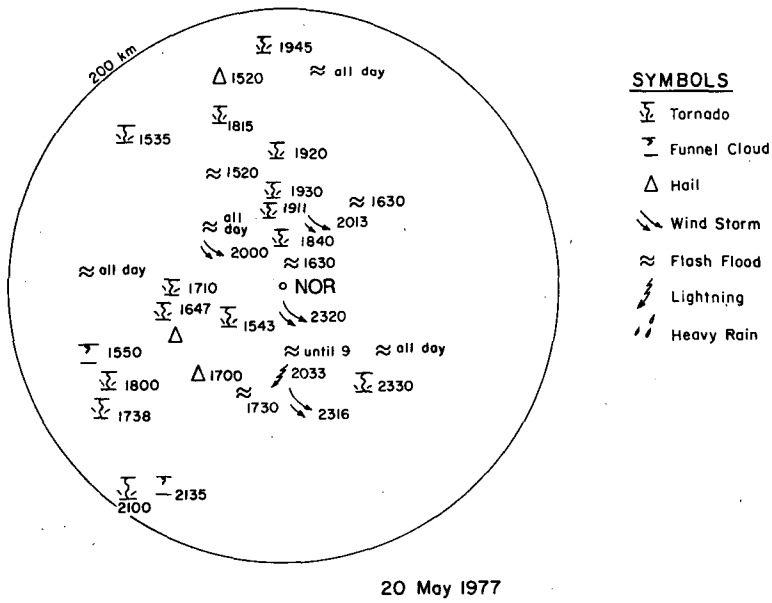

FIG. 4. Severe weather map example. Severe weather reports occurring within study area (enclosed by circle) on 20 May 1977 (local-midnight to local-midnight) are plotted according to key. Times (CST) next to severe-weather symbols correspond to time of the event. UTC = CST + 6 h.

for the various categories of underlying radar-echo structure.

f. Sounding data

To address the environmental conditions supporting major rain events in a more quantitative fashion, standard synoptic soundings taken at Oklahoma City (near the center of the study area) twice daily (00 and 12 UTC) were obtained from a 40-year archive of North American upper-air data maintained by the NOAA Forecast Systems Laboratory. Thermodynamic data in this archive originated from the National Climatic Data Center (NCDC). Accompanying wind data for study years 1977–80 were subject to vertical smoothing routinely employed by NCDC. For study years 1981 and 1982, however, wind data recorded in real-time (as transmitted by the National Weather Service) had been substituted in the archive. These winds were not subjected to smoothing and thus provided a somewhat better description of sharp vertical shears and speed maxima.

As will be discussed in section 8, the soundings were divided into groups corresponding to various types of observed radar echo organization. Once grouped, they were examined individually to acquire initial impressions regarding similarities and differences among the groups. Soundings were then located more precisely with respect to the radar echo patterns and checked for signs of contamination by local effects (e.g., entrainment into convective updrafts). Those soundings deemed unrepresentative of the ambient conditions on the low-level inflow side of the corresponding mesoscale convective system were eliminated. When multiple mesoscale precipitation systems passed through the study area during a 12-h period between observations, a given sounding was assumed to represent only the first storm that passed subsequent to its release; additional systems prior to the next observation time were thus eliminated from this part of the study. In several cases, systems were spaced so closely together that the inflow into a storm appeared to have been appreciably modified by the preceding system. In these instances, although the sounding profile may have been "disturbed," it was nonetheless assumed to represent conditions immediately ahead of the subsequent storm and was thus retained for analysis.

Some processing of the data was required prior to constructing average soundings for the various categories of radar echo organization. Mandatory and significant-level data were interleaved for each sounding and subsequently interpolated to levels spaced 25 mb apart from the surface to 100 mb; surface values were retained without alteration. Subsequently, soundings were averaged to determine mean properties for each of the groups and to allow ready comparison of their respective wind and thermodynamic profiles. Various routine parameters (e.g., stability indices, measures of mean wind and vertical shear through various layers, etc.) were derived for each sounding. Averages of these parameters for all constituent soundings in each group were then computed so that differences in the environments of systems exhibiting contrasting radar echo or-

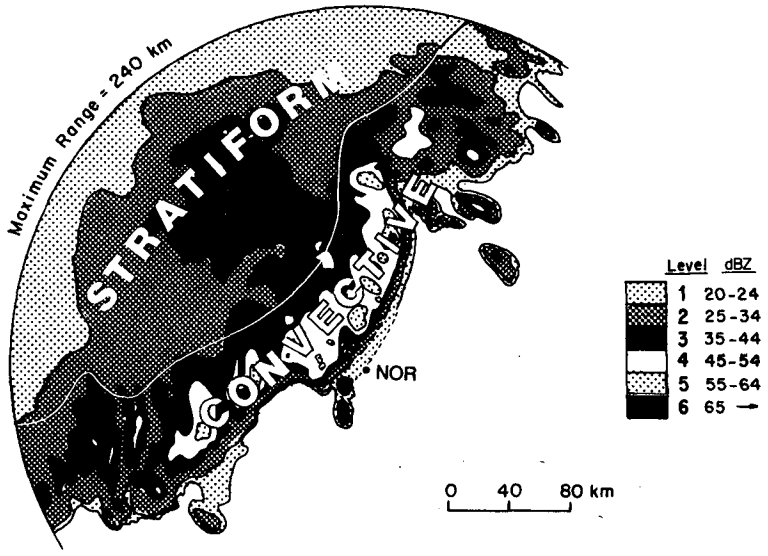

FIG. 5. Example of the partition of convective and stratiform echo. Shaded reflectivity pattern (dBZ values according to key at lower right) is derived from low-elevation plan-position indicator photograph from the NSSL WSR-57 radar at 0240 UTC 17 May 1982. Arc corresponds to 240 km range circle centered on radar. Reflectivity values (dBZ) corresponding to levels of shading are given in key. Horizontal distance scale (km) is indicated (north toward top of page).

ganization could be quantified and tested for statistical significance.

3. Occurrence of stratiform precipitation in major rain events

Studies of mesoscale convective systems in the tropics have shown that as the larger cloud systems grow and mature, they develop a mesoscale area of stratiform rain that falls from a widespread cloud shield extending over the whole system (Houze and Betts 1981). Midlatitude warm season rainstorms appear to behave in a similar manner. Maddox (1980) noted that the largest and most intense mesoscale convective complexes were characterized by stratiform rain in their mature and dissipating stages.[1] As noted in the Introduction, case studies of midlatitude squall lines also indicate that areas of lighter, more stratified precipitation tend to accompany the convection in these storms, either to the rear or toward the northern ends of the convective lines.

To ascertain whether the development of stratiform precipitation in conjunction with convective storms is a regularly occurring feature of the midlatitude warm season rainstorms, the radar data throughout the 24-h period of each major rain event was examined to determine the presence or absence of stratiform precipitation. To distinguish convective from stratiform rain areas, a *convective echo region* was defined as:

- a region 20–50 km in horizontal dimension with reflectivity peaks of at least two contour levels over a horizontal distance of 10 km and contour shapes that varied spatially on a scale $\leq$ 10 km and temporally over periods $\leq$ 1 h.

Specifying that the contour shapes vary spatially on a fine scale avoids having large-scale, more homogeneous echoes being classified as convective because they have a tight gradient of reflectivity at their edges. The definition above is generally consistent with echo-identification criteria used previously by Houze (1973), Cheng and Houze (1979), and Churchill and Houze (1984).

The definition for a *stratiform echo region* follows as:

- any nonconvective echo on a scale of 40 km or more.

The scale requirement in this definition excludes such phenomena as weak isolated showers, dissipating stratiform fragments, gust front or "fine-line" echoes, and the effects of anomalous electromagnetic wave propagation.

Figure 5 is a tracing of the photograph of the NSSL radar scope at 0240 UTC 17 May 1982. The outlined convective and stratiform areas were determined sub-

[1] While Maddox did not refer to stratiform precipitation explicitly, his descriptions (viz. "a large region of weaker echo," "an initial burst of heavy rain . . . followed by more than 4½ h of light rain," etc.) are wholly consistent with the presence of stratiform cloud and precipitation.

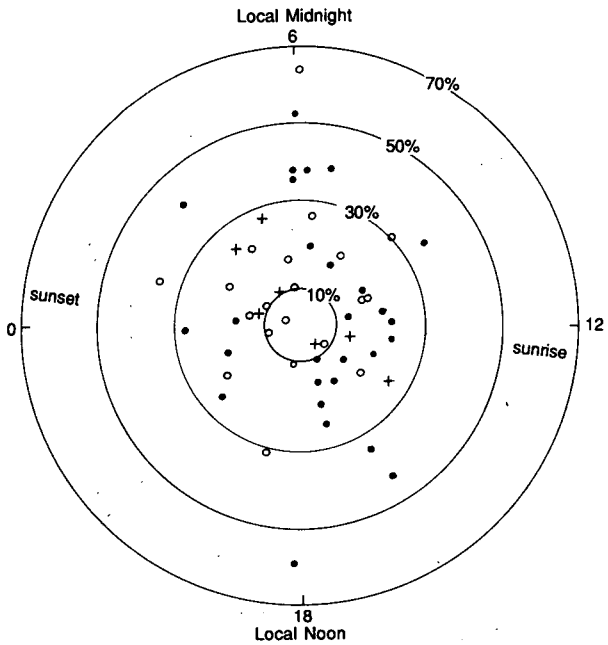

FIG. 6. Polar coordinate plot of times (UTC) of maximum stratiform echo coverage during Major Rain Events. Radius corresponds to size of stratiform echo in terms of percentage (%) of the study area covered; angle denotes time of its occurrence. Solid circles denote cases with complete radar data; open circles denote cases with incomplete radar data judged adequate for a reliable estimate of echo properties; plus symbols denote dubious estimates of echo properties due to paucity of radar data.

jectively but in accordance with the criteria stated above.

All the available radar data for major rainfall events were examined. To determine the sizes of stratiform echo areas, the data were sampled at least every 2 h, and the regions of stratiform echo were identified and measured with a planimeter. The maximum percentage of area covered by stratiform echo and the time that maximum occurred were noted for each case. If the data were incomplete and there was doubt that the maximum was reached before scope photography ceased, then that case was noted as missing some data. Four of the 55 major rain events were thus eliminated ("Stratiform Echo Coverage" indicated as missing by "M" in Table 2), yielding 51 days on which the radar data could be examined thoroughly.

One of the preeminent results indicated by Table 2 is that nearly every major rain event for which adequate radar data were available exhibited stratiform radar echo over a large portion of the study area at some time during the storm. Of the 51 cases for which radar data were available, 48 attained $\geq 10\%$ coverage of the study area by stratiform echo (10% coverage of the study area corresponds to about 12 500 km^2), and 24% (or 30 100 km^2) was the average stratiform coverage reached in these storms.

The times of maximum stratiform echo occurrence during each major rain event are indicated in Table 2 and plotted in Fig. 6. No strongly preferred time of day for maximum stratiform echo coverage is evident. However, a slight preference for extremely large stratiform areas (covering >30% of the study area) to occur in the middle of the night (0300–0900 UTC), with a peak near local midnight (0600 UTC), is suggested. The smaller maximum stratiform regions (covering <30% of the study area) had a slight tendency to be less frequent in early afternoon, around 1900 UTC.

4. Relationship of stratiform and convective precipitation areas in individual mesoscale precipitation systems

In the preceding section it was established that large stratiform rain areas are a regularly occurring feature of major springtime rain events in central Oklahoma. However, this stratiform precipitation is generally accompanied by numerous convective cells, and the relationship of the stratiform rain to the pattern of convective cells is a signature of the mesoscale organization of the parent storm. For example, case studies of mesoscale convective systems in both the tropics and midlatitudes suggest that stratiform precipitation often (though not always) develops as an outgrowth of deep convection to the rear of a moving line of convective cells. As a way of beginning a systematic investigation of the spatial arrangement of stratiform and convective precipitation areas in the 51 major rain events for which comprehensive radar data were available, we made a preliminary examination of the echo patterns to determine how frequently a mesoscale precipitation system consisting of a line of convective cells followed by a region of stratiform rain could be identified.

The result of this survey was that only about 20% of the individual mesoscale precipitation systems observed during major rain events could be identified as having organized mesoscale structure as sharply defined as that described in previously published case studies. However, a much larger number of storms appeared to resemble those cases partially. Among the most clearly defined cases, several common features were noted which suggested the following ten basic characteristics of *leading-line/trailing-stratiform organization:*

The leading *convective line* has:

1) Arc shape (convex toward the leading edge)

2) Generally northeast-southwest orientation. (This was variable: some lines were nearly north–south while others were nearly east–west.)

3) Rapid movement with an eastward and/or southward component (>10 m s^{-1} in a direction normal to the line orientation).

4) Solid appearance (a series of intense reflectivity cells solidly connected by echo of more moderate intensity).

5) Very strong reflectivity gradient at leading edge (i.e., gradient much stronger at leading edge than back edge of the convective region).

6) Serrated leading edge (leading edge of echo is jagged, with forward-extending protrusions at an apparent wavelength of ≈5–10 km).

7) Elongated cells oriented 45–90° with respect to line (elongated cells appear to be related to the serrated leading edge).

The trailing *stratiform region* has:

8) Large size (over 10^4 km^2 in horizontal area).

9) A notch-like concavity at rear edge (believed to be associated with mesoscale inflow of dry air that erodes a portion of the stratiform echo; see Smull and Houze 1985, 1987b).

10) A secondary maximum of reflectivity (separated from the convective line by a narrow channel of lower reflectivity).

Two possible manifestations of these ten characteristics are illustrated by the schematic radar echo patterns presented in Figs. 7 and 8. The organization shown in Fig. 7 is referred to as the *Symmetric Case,* while that in Fig. 8 is referred to as the *Asymmetric Case.*

In the *Symmetric Case,* the convective line shows

- no preference for the most intense cells to be found at any particular location along the line. New cell growth apparently occurs all along the leading edge of the line while the stratiform region has its

- centroid located directly behind the center of the convective line.

In the *Asymmetric Case,* the convective line is

- stronger on its southern, southwestern, or western end. That is, younger, newly formed, and more intense cells are located toward one end of the line, while weaker, dying cells on the verge of becoming stratiform are found toward the other end of the line and the centroid of the stratiform region is:

- biased toward the north, northeast, or east end of the line rather than centered behind the line.

Figure 9 shows six examples of clearly defined leading-line/trailing-stratiform organization that span the spectrum from Symmetric to Asymmetric structure. Figures 9a–c contain particularly good examples of Symmetric structure, while the echo pattern in Fig. 9f is an especially good example of the Asymmetric type of structure. The methodology used to classify mesoscale precipitation systems (and thereby identify the examples shown) will be described in section 5.

In addition to echo patterns that closely or partially resembled either the Symmetric or Asymmetric Case, our preliminary survey revealed a significant number of mesoscale precipitation systems whose echo patterns bore no apparent resemblance to either. These storms

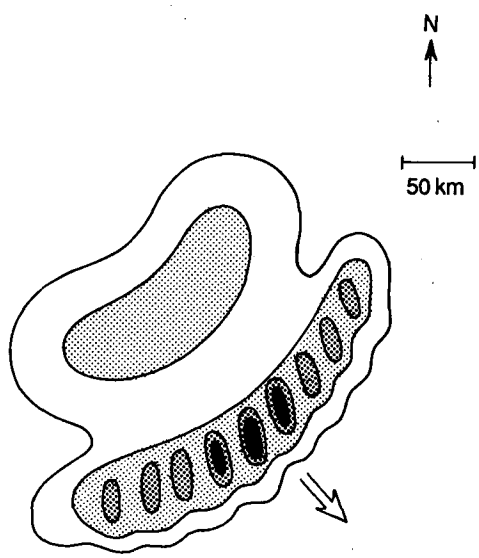

FIG. 7. Schematic depicting Symmetric type of leading-line/trailing-stratiform mesoscale precipitation system organization. Large vector indicates direction of system motion. Levels of shading denote increasing radar reflectivity, with most intense values corresponding to convective cell cores. Horizontal scale and north arrow are shown.

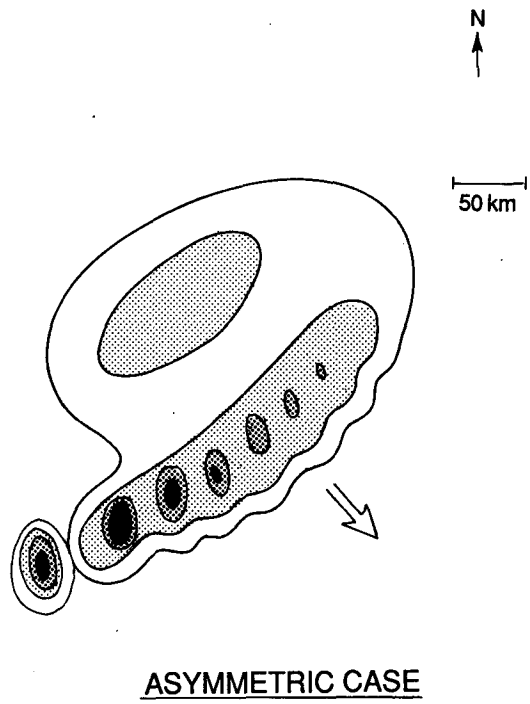

FIG. 8. As in Fig. 7 except for Asymmetric type of leading-line/trailing-stratiform mesoscale precipitation system organization.

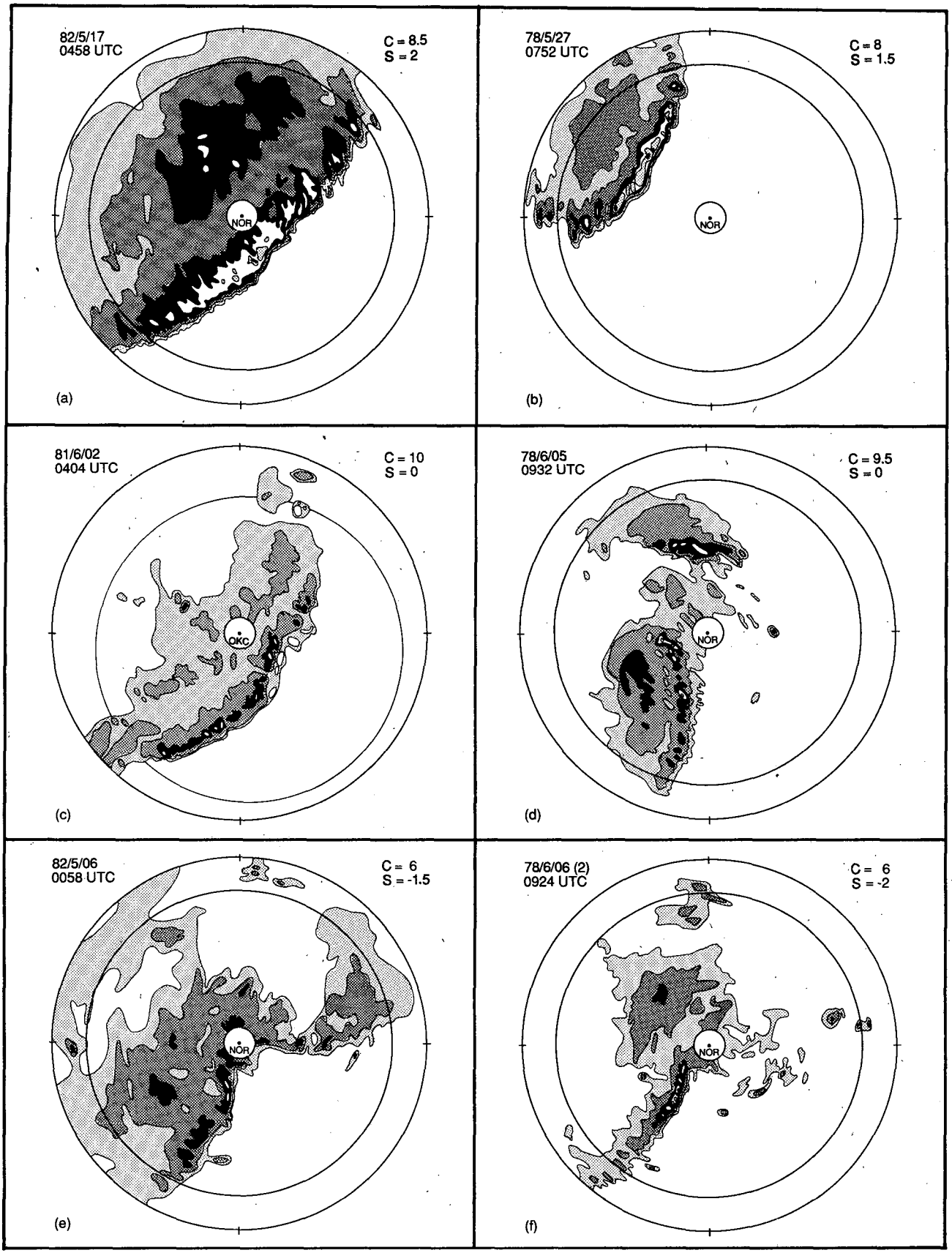
82/5/17
0458 UTC
C = 8.5
S = 2
NOR
(a)
78/5/27
0752 UTC
C = 8
S = 1.5
NOR
(b)
81/6/02
0404 UTC
C = 10
S = 0
OKC
(c)
78/6/05
0932 UTC
C = 9.5
S = 0
NOR
(d)
82/5/06
0058 UTC
C = 6
S = -1.5
NOR
(e)
78/6/06 (2)
0924 UTC
C = 6
S = -2
NOR
(f)

have been retained in our study along with the others and are referred to as *Unclassifiable* cases. They are unclassifiable in the sense that their mesoscale organization bore no resemblance to the idealized radar echo patterns in Figs. 7 or 8. They should not be interpreted as insignificant or uninteresting, rather only as exhibiting a different type of radar-echo structure than that embodied in Symmetric Case and Asymmetric Case models. They contribute significantly to major rain events, always containing large stratiform areas at some stage of their existence and often producing severe weather. The patterns of convection in the Unclassifiable systems often were wild and chaotic, and the location of the stratiform rain exhibited no typical relation to the convective cells. Some examples of radar echo patterns in Unclassifiable cases are shown in Fig. 10.

5. Tabulation of characteristics of mesoscale precipitation systems

To make our determination of the type and degree of storm organization occurring during the 51 radar-documented major rain events more precise, we surveyed all the radar data again, this time tabulating systematically the degree to which the radar echo patterns for each event resembled the archetypes described in the preceding section. This procedure was repeated several times, always with two of the authors simultaneously viewing the data, checking and rechecking evaluations made during previous passes through the data.

For each major rain event, the radar echo patterns were subdivided into distinct mesoscale precipitation systems (MPSs). Each MPS was critically examined to determine if it possessed the structural characteristics of the Symmetric Case, Asymmetric Case, or Unclassifiable type of organization. If more than one MPS contributed significantly to the precipitation in a major rain event, then the structure of each mesoscale system was evaluated and recorded separately. Of the 51 major rain events, 33 were affected primarily by one MPS, 13 were affected by two MPSs, one was affected by three MPSs, and one was affected by four separate MPSs. In one instance, three MPSs were spread over two successive major rain events. Thus, the radar echo patterns of a total of 69 MPSs that occurred during the 51 major rain events were surveyed and evaluated for their resemblance (or otherwise) to the Symmetric, Asymmetric, or Unclassifiable archetype.

Details pertaining to the application of the classification scheme are given in the Appendix, but the gist of the technique is as follows. A matrix was constructed (Table A1 in the Appendix) in which each row corresponded to one of the 69 MPSs and each column corresponded to one of the characteristics of leading-line/trailing-stratiform (ll/ts) precipitation structure enumerated in section 4. (Additional data regarding severe weather reports, MCC characteristics, etc. associated with each MPS were also listed.) Each MPS was identified by the date of the particular major rain event (as in Table 2) during which it occurred. In those major rain events where multiple MPSs passed over the study area during the 24-h period, systems were denoted by (1), (2), . . . , following the date in the order of their appearance.

For a small number of cases, the quality of the radar data was so low as to preclude detailed evaluation of precipitation structure; no attempt was made to classify echoes during these major rain events, and they were designated as "Bad Data" in Table A1. As alluded to previously, some MPSs bore so little resemblance to either the Symmetric or Asymmetric type of ll/ts organization that no attempt was made to evaluate the extent to which the individual characteristics of ll/ts structure were present. Such systems are listed as "Unclassifiable" in Table A1. For the remaining MPSs, which to varying degrees resembled the ll/ts archetype, two scores were calculated to quantify and categorize their structure:

C A measure of the storm's resemblance to the leading-line/trailing-stratiform archetype (i.e., its "classifiability"), defined by the presence or absence of the ten basic characteristics listed in section 4.

Values of C may range from −10 to 10; a value of 10 indicates the maximum possible degree of leading-line/trailing-stratiform structure that can be shown by our system of evaluation. The second quantity addresses the particular type of ll/ts organization that was present:

S A measure of the resemblance to either the Symmetric or Asymmetric type of ll/ts organization, defined by the location of new cell growth and the

FIG. 9. Six examples (a–f) of Strongly Classifiable leading-line/trailing-stratiform organization, ranging from Symmetric to Asymmetric. Shaded reflectivity patterns (levels of shading as in Fig. 5, corresponding to dBZ values in Table 1) drawn from low-elevation (typically 0.8°) plan-position indicator photographs. Mesoscale Precipitation System designator (as in Table A1) and time (UTC) of radar data are shown in upper left-hand corner; times later than 1800 UTC correspond to previous day, in accordance with Major Rain Event definition (see text). Outermost circle denotes 240 km range from radar ("OKC" in panel c denotes National Weather Service radar at Oklahoma City; "NOR" in all other panels denotes NSSL WSR-57 at Norman). Registration marks on outermost circle are at 90° azimuth intervals (north toward top of page). Innermost 20 km range circle denotes intense ground-clutter zone within which precipitation-echo structure could not be determined. Intermediate circle (200 km radius) outlines study area. "C" and "S" scores corresponding to echo pattern (from Table A1, described in text) are shown in upper right-hand corner.

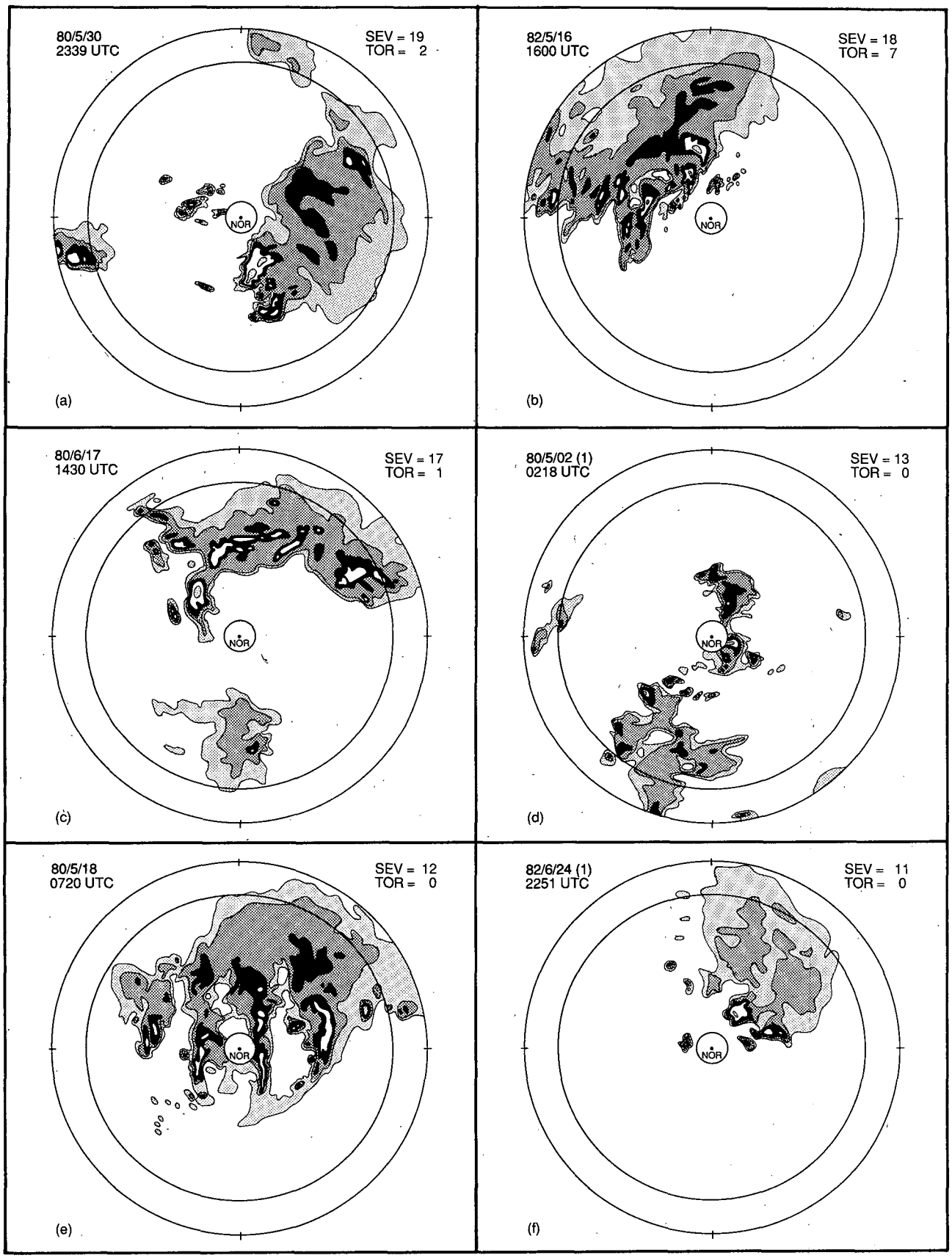

FIG. 10. As in Fig. 9, except for ten examples (a–j) of Unclassifiable mesoscale precipitation system structure sorted in order of decreasing number of severe weather reports. Total number of severe weather reports (all types) and number of tornadoes reported during system passage ("SEV" and "TOR," respectively, from Table A1) are indicated.

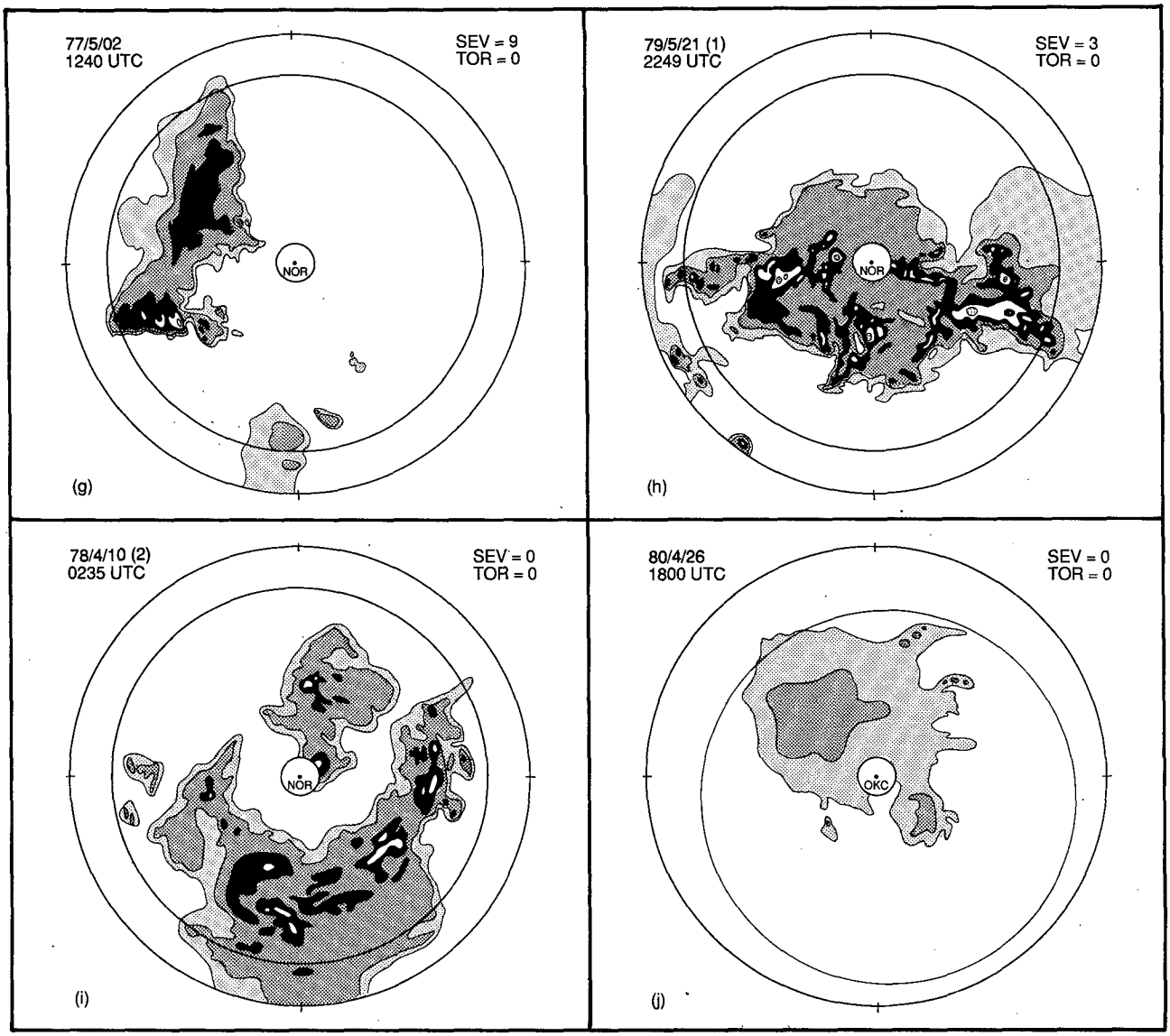

FIG. 10. (*Continued*)

centroid of the stratiform region *vis a vis* the convective line, as described in section 4.

Values of S may range from −2 to 2. Positive values of S indicate similarity to the Symmetric case, while negative values indicate similarity to the Asymmetric Case.

The detailed results of these tabulations for all 69 MPSs are listed in Table A1. Six of those systems were characterized by "Bad Data" and thus their radar-echo structure could not be evaluated. Of the remaining 63 mesoscale systems, 21 were found to be "Unclassifiable" while 42 were found to be "Classifiable," i.e. they exhibited at least some degree of ll/ts radar-echo structure. Classifiable MPSs have been divided into nine categories depending upon their C and S scores. The number of MPSs in each of these categories (as well as for Unclassifiable systems) is summarized in Table 3. It can be seen that 14 cases had $C > 5$, indicating *strong* tendency toward ll/ts organization, 18 had C values ranging from 0–5, indicating a *moderate* tendency to ll/ts organization, and 10 had $C < 0$, indicating only a *weak* resemblance to ll/ts organization. Within each of these three C-categories, we further discriminated (based upon the S-score) whether the particular echo organization was more similar to the Symmetric Case ($S \geq 1$) or the Asymmetric Case ($S \leq -1$). Values of S between 1 and −1 may be considered as intermediate between Symmetric and Asymmetric structure. In each of the C categories (strong, moderate

TABLE 3. Number of mesoscale precipitation systems (MPSs) in each category of mesoscale radar-echo organization (described in text) during the study period (April–June 1977–1982).

Degree of organization	Range of scores	Type of organization: Symmetric $S \geq 1$	Intermediate $-1 < S < 1$	Asymmetric $S \leq -1$	All types All S
Strongly Classifiable	$C > 5$	4	7	3	14
Moderately Classifiable	$0 \leq C \leq 5$	6	6	6	18
Weakly Classifiable	$C < 0$	1	3	6	10
All Classifiable systems	All C	11	16	15	42
All Unclassifiable systems					21

and weak), the S values were spread rather evenly among Symmetric, Asymmetric and Intermediate categories (cf. Table 3).

Tables 3 and A1 strongly indicate that the radar echo patterns associated with springtime rainstorms over Oklahoma are quite variable and constitute a continuum of mesoscale organization. When ll/ts structure occurs, it may range in degree from crisp, obvious clarity in some cases to only a weakly suggested tendency in others. Moreover, when ll/ts structure is present, whether strongly or only weakly, the degree to which the structure resembles the Symmetric or Asymmetric model also varies over a continuum.

The unique character of the Unclassifiable MPSs (denoted "U" in Table A1) rests not only in their distinctive mesoscale radar-echo structure; they also appear to differ from the Classifiable systems in terms of their accompanying severe weather and environmental properties. These aspects will be elaborated upon in sections 6 and 8.

Several of the MPSs considered here have been the subject of detailed case studies reported in the literature. Those of which we are aware (identified by their entry in column A of Table A1 and the corresponding citation) are: 77/5/20—Kessinger et al. (1987); 79/5/03(1)—Heymsfield and Schotz (1985); and 79/5/21(1)—Watson et al. (1988). In addition, as mentioned in the Introduction, studies of the formation of severe and non-severe squall lines over Oklahoma (a number of which contributed to the major rain events discussed here) have been undertaken by Bluestein and Jain (1985) and Bluestein et al. (1987).

6. Occurrence of severe weather during major rain events

In previous sections, it has been shown that major springtime rain events in Oklahoma are typically characterized by organized mesoscale precipitation systems (MPSs) that develop large areas of stratiform precipitation arranged in various configurations with respect to areas and lines of convective cells. But springtime in Oklahoma is also a season of severe weather, and one might ask: To what extent does severe weather occur in association with the major rain events? Moreover, is severe weather occurrence related to the categories of mesoscale radar-echo organization discussed in section 5? To explore these questions, we transferred reports from our severe weather maps (e.g., Fig. 4) onto the radar reflectivity displays for each storm so that they might be interpreted in terms of both their location with respect to echo pattern and relationship to the life cycle of individual MPSs.

a. Climatology

A summary of the severe weather reported over the entire study period is given in Table 4. Depending on the type, 32%–66% of the severe weather reports occurred during major rain events. Summation over all types indicates that 481 of the 971 total severe weather reports occurred during these events. That is, roughly half of Oklahoma's springtime severe weather occurred in association with significant precipitation, while the other half arose from storms failing to produce widespread heavy rainfall. A future study should attempt to distinguish the meteorological differences between the severe weather associated with isolated convection and that generated in major rainstorms, which are addressed here.

To illustrate the seasonal variation of reports during the 1977–82 study period, the histograms in Figs. 11 and 12 subdivide the three study months, April–June, into nine 10-day periods.[2] Moreover, during each major rain event some of the severe weather reports were associated with isolated echoes (e.g., convective cells occurring prior to the appearance, ahead, or in the wake of MPSs) while the remainder were embedded within the contiguous mesoscale precipitation systems (as defined in section 2b) that accounted for most of the rain over the study area. By overlaying the severe weather maps on the radar echo patterns, we were able to make this distinction. (Note that no such distinction was

[2] Each subdivision consists of a block of ten 24-h periods running from local noon-to-noon (CST), the first and last of which end at noon on the indicated dates. This follows the convention employed in designating major rain events.

TABLE 4. Severe weather reports during entire study period (April–June 1977–82).

Measure	Tornadoes	Funnel clouds	Hail	Wind	Lightning	Floods	Heavy rain	All types
Reports logged during major rain events	80	63	125	100	17	84	12	481
Reports for all days (regardless of rainfall)	168	178	235	189	53	127	21	971
Percentage of reports during major rain events	48	35	53	53	32	66	57	50

made in Table A1.) The tallies shown in Fig. 11 thus distinguish (1) the total number of severe weather reports observed during each 10-day period, (2) the subset of those reports that occurred during major rain events, and (3) the subset of reports during major rain events that were located within MPSs. When summed over the entire study period, the data in Fig. 11 indicate that the vast majority (428 of 481, or 89%) of the severe weather reported during major rain events was located within the contiguous, horizontally extensive radar echo boundaries of MPSs.

The severe weather data are further subdivided according to type (i.e., tornadoes, wind damage, etc.) in Fig. 12. In addition to columns representing the total number of reports and those associated with major rain events, the partition of reports between the convective and stratiform regions in MPSs (cf. Fig. 5) is also shown for each 10-day period in Figs. 12a–g. It was sometimes impossible to locate a report accurately within a MPS (e.g., if a vague time such as "evening" or "all night" was used to describe the event); for this reason, the sum of all severe reports located in stratiform and convective regions may be slightly less than the number designated as "located in MPSs" for the corresponding 10-day period shown in Fig. 11. This is especially true of flood reports, whose durations were typically much longer (and specified less precisely) than those of other severe weather types.

Figure 12 shows that the majority of severe weather reports located within MPSs were associated with their convective regions. However, this was less true for flood reports, which were more evenly divided between convective and stratiform echo regions. This result is not unexpected since the peak runoff responsible for some flooding tends to lag the heavy (convective) rain by several hours, thus coinciding with the passage of a stratiform area. (In a few cases, flooding may have occurred along streams swollen in response to distant heavy rains.) Persistent light rainfall associated with passage of the stratiform region could also have exacerbated flooding initiated by the earlier or distant convective cells.

Tornado and hail reports were biased toward the early stages of MPS development, and were most frequently associated with (1) cells located toward the southern ends of squall lines, and (2) isolated strong cells ahead of squall lines. (Because they lay outside the MPSs, reports of the latter variety were not included in the "Reports located in MPS convective echo" columns of Fig. 12; they were, however, included in the columns designated "Reports during MREs.") High wind reports sometimes accompanied isolated severe cells, but were more numerous along well-developed convective lines. Some tendency for these wind reports to be associated with bow-shaped portions of mature squall lines (e.g., Fujita 1981; Johns and Hirt 1987) was noted. Little significance could be attributed to reports of heavy rain apart from their consistent association with convective cells.

The virtually exclusive association of lightning reports with the convective regions of MPSs implied by Fig. 12e may seem somewhat surprising in view of Zipser's (1983) observation that the stratiform regions of mesoscale convective systems are often characterized by frequent thunder. However, the lightning reported in *Storm Data* is only that which inflicts damage, and is thus confined to the effects of cloud-to-ground strokes. Although electrification of the stratiform regions of MPSs is receiving increased attention (e.g., Rutledge and MacGorman 1988), recent findings indicate that the number of cloud-to-ground discharges is dominated by the convective regions of these storms. Widespread thunder emanating from stratiform regions, as described by Zipser, is thought to be primarily due to intracloud lightning.

The seasonal variation of overall severe weather occurrence (Fig. 11) generally follows that of the major rain events (cf. Fig. 3). The peak occurrence appears to be around May 20. A secondary peak in severe

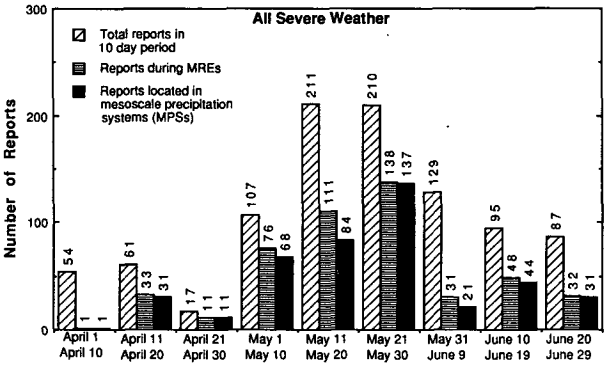

FIG. 11. Histogram showing frequency distributions by 10-day intervals of: total number of severe weather reports (all types, diagonally-hatched columns); reports occurring during Major Rain Events (darker, horizontally-hatched columns); and reports located within radar echo of Mesoscale Precipitation Systems (black columns).

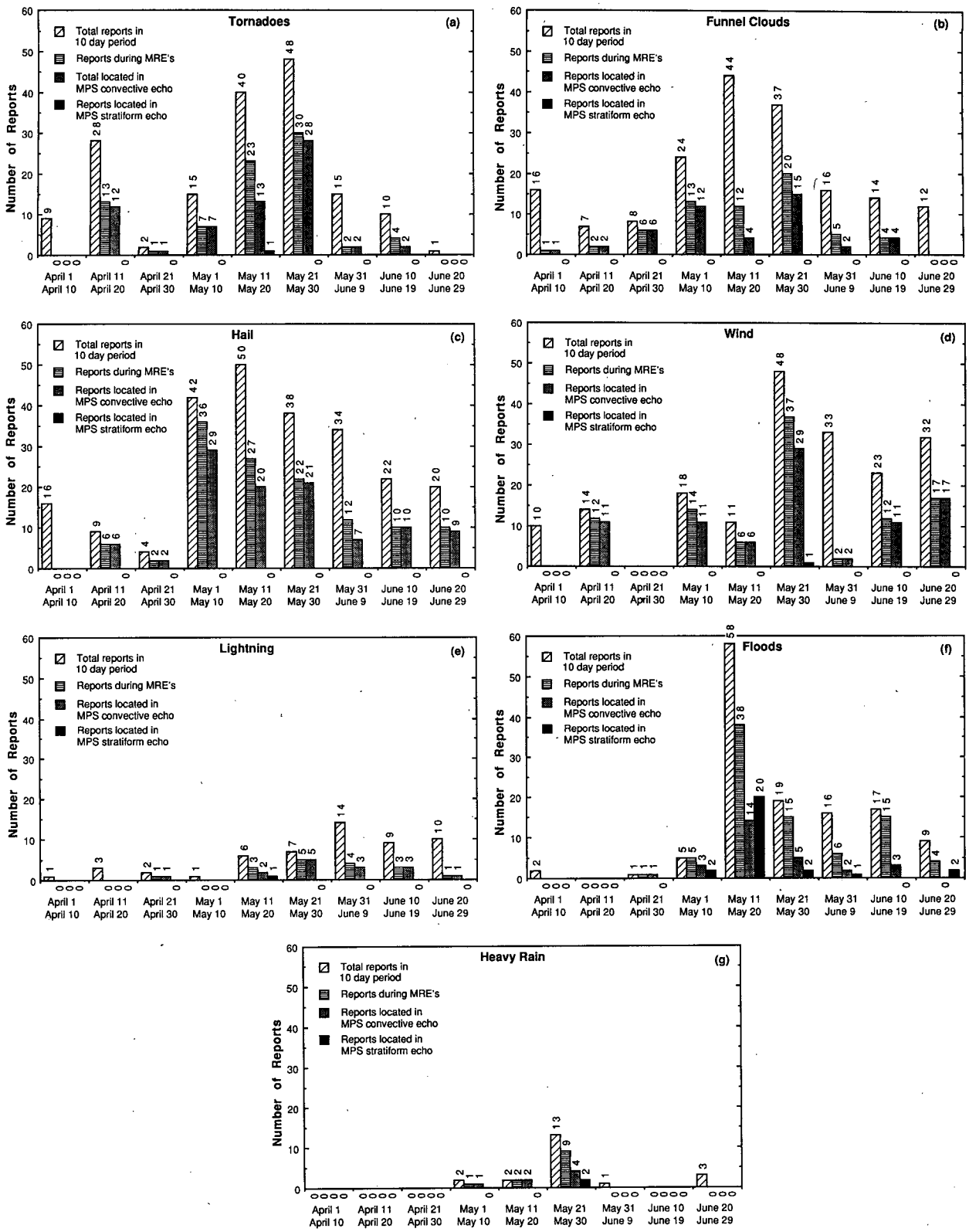

FIG. 12. Histograms showing frequency distributions by 10-day intervals of severe weather reports subdivided by type (a–g). Data shown are: total reports during interval (diagonally-hatched columns); reports occurring during Major Rain Events (darker, horizontally-hatched columns); reports located within Mesoscale Precipitation System (MPS) convective echo (stippled columns); and reports located within MPS stratiform echo (black columns).

weather is seen in mid-April. Figure 12 indicates how each of the seven types of severe weather contributed to the total frequency shown in Fig. 11; for example, Fig. 12 shows that the April maximum of severe weather appeared most strongly in tornadoes, and to a lesser degree in hail and wind damage. It has been noted that the peak occurrence of tornadoes in the United States is in the period May–June, but that "violent" tornadoes are most common in March–April, while "strong" tornadoes (less violent) peak in May–June (Fig. 4 of Kelly et al. 1978). This observation, together with Figs. 11 and 12, indicates that the secondary April maximum of severe weather over the study area may be associated with a somewhat different type of convective storm than the major peak in late May.

Figure 12 further suggests that the character of the convection associated with major rain events underwent other transitions as the season progressed. The date of peak severe weather occurrence (disregarding the secondary maximum for tornadoes) was earliest for funnel clouds, hail, and floods (11–20 May), followed by tornadoes, wind damage, and heavy rain (21–30 May), and finally lightning (31 May–9 June). Whether this sequence represents a typical seasonal transition in the nature of convective systems producing severe weather in central Oklahoma or is a sampling fluctuation characteristic only of this particular six-year period is uncertain and should be tested using a larger and independent data sample.

b. Occurrence of severe weather in relation to mesoscale radar-echo structure

From the listing of severe weather reports for each MPS in Table A1, it is possible to relate frequency of

TABLE 5. In (a) and (b), severe weather (all types) recorded in the study area during Major Rain Events (defined in text) as a function of category of mesoscale radar echo organization of the associated Mesoscale Precipitation System (MPS). (a) Total number of severe weather reports. (b) Average number of reports per MPS, i.e. total number reports normalized by number of responsible MPSs. In (c), number of MPSs with ≥ 10 severe weather reports.

(a)

		Type of organization			
Degree of organization	Range of scores	Symmetric $S \geq 1$	Intermediate $-1 < S < 1$	Asymmetric $S \leq -1$	All types All S
Strongly Classifiable	$C > 5$	66	32	8	106
Moderately Classifiable	$0 \leq C \leq 5$	14	15	95	124
Weakly Classifiable	$C < 0$	0	5	72	77
All Classifiable systems	All C	80	52	175	307
All Unclassifiable systems					161

(b)

		Type of organization			
Degree of organization	Range of scores	Symmetric $S \geq 1$	Intermediate $-1 < S < 1$	Asymmetric $S \leq -1$	All types All S
Strongly Classifiable	$C > 5$	16.5	4.6	2.7	7.6
Moderately Classifiable	$0 \leq C \leq 5$	2.3	2.5	15.8	6.9
Weakly Classifiable	$C < 0$	0	1.7	12.0	7.7
All Classifiable systems	All C	7.3	3.3	11.7	7.3
All Unclassifiable systems					7.7

(c)

		Type of organization			
Degree of organization	Range of scores	Symmetric $S \geq 1$	Intermediate $-1 < S < 1$	Asymmetric $S \leq -1$	All types All S
Strongly Classifiable	$C > 5$	2	1	0	3
Moderately Classifiable	$0 \leq C \leq 5$	0	0	4	4
Weakly Classifiable	$C < 0$	0	0	2	2
All Classifiable systems	All C	2	1	6	9
All Unclassifiable systems					8

TABLE 6. Average number of severe weather reports per Mesoscale Precipitation System (MPS), i.e. total reports normalized by number of responsible MPSs, subdivided by type of report. (a) Tornadoes; (b) Funnel clouds; (c) Hail; (d) High wind; (e) Lightning; (f) Flooding; and (g) Heavy Rain.

		Type of organization			
Degree of organization	Range of scores	Symmetric $S \geq 1$	Intermediate $-1 < S < 1$	Asymmetric $S \leq -1$	All types All S
		(a) Tornadoes			
Strongly Classifiable	$C > 5$	2.3	0.6	0.3	1.0
Moderately Classifiable	$0 \leq C \leq 5$	0.2	0	3.3	1.2
Weakly Classifiable	$C < 0$	0	0	4.3	2.6
All Classifiable systems	All C	0.9	0.3	3.1	1.5
All Unclassifiable systems					0.9
		(b) Funnel Clouds			
Strongly Classifiable	$C > 5$	2.8	0.7	0	1.1
Moderately Classifiable	$0 \leq C \leq 5$	1.0	0.2	2.3	1.2
Weakly Classifiable	$C < 0$	0	0	1.0	0.6
All Classifiable systems	All C	1.6	0.4	1.3	1.0
All Unclassifiable systems					0.9
		(c) Hail			
Strongly Classifiable	$C > 5$	1.3	1.3	0.3	1.1
Moderately Classifiable	$0 \leq C \leq 5$	0.2	0.7	4.3	1.7
Weakly Classifiable	$C < 0$	0	0.3	2.0	1.3
All Classifiable systems	All C	0.6	0.9	2.6	1.4
All Unclassifiable systems					3.0
		(d) High Wind			
Strongly Classifiable	$C > 5$	4.0	0.7	0	1.5
Moderately Classifiable	$0 \leq C \leq 5$	0	1.3	2.8	1.4
Weakly Classifiable	$C < 0$	0	1.3	3.0	2.2
All Classifiable systems	All C	1.5	1.1	2.3	1.6
All Unclassifiable systems					1.5
		(e) Lightning			
Strongly Classifiable	$C > 5$	1.0	0.1	0	0.4
Moderately Classifiable	$0 \leq C \leq 5$	0.2	0.3	0.3	0.3
Weakly Classifiable	$C < 0$	0	0	0.2	0.1
All Classifiable systems	All C	0.5	0.2	0.2	0.3
All Unclassifiable systems					0.1
		(f) Flooding			
Strongly Classifiable	$C > 5$	5.3	0.9	2.0	2.4
Moderately Classifiable	$0 \leq C \leq 5$	0.8	0	2.2	1.0
Weakly Classifiable	$C < 0$	0	0	1.5	0.9
All Classifiable systems	All C	2.4	0.4	1.9	1.4
All Unclassifiable systems					1.0

severe weather occurrence to the type of observed radar-echo structure. Table 5 summarizes the total number of severe weather reports in each of the nine categories of classifiable mesoscale radar-echo structure described in section 5. Its format is similar to that of Table 3, in which the frequency of occurrence of MPSs in each category of organization is indicated. Table 5a presents the total number of severe weather reports for the six-year study period. As mentioned previously, 481 severe weather reports were logged during major rain events.

TABLE 6. (*Continued*)

Degree of organization	Range of scores	Type of organization: Symmetric $S \geq 1$	Intermediate $-1 < S < 1$	Asymmetric $S \leq -1$	All types All S
		(g) Heavy Rain			
Strongly Classifiable	$C > 5$	0	0.3	0	0.1
Moderately Classifiable	$0 \leq C \leq 5$	0	0	0.5	0.2
Weakly Classifiable	$C < 0$	0	0	0	0
All Classifiable systems	All C	0	0.1	0.2	0.1
All Unclassifiable systems					0.3

Of these reports, 307 were associated with Classifiable mesoscale radar-echo structure, while 161 occurred in connection with Unclassifiable MPSs. (The remaining 13 were reported during major rain events characterized by "Bad Data," which are excluded from Table 5.) Severe weather data for Classifiable systems are further stratified according to their values of C (degree of leading-line/trailing-stratiform structure) and S (similarity to Symmetric or Asymmetric Case). Three of the nine basic categories produced most of the reported severe weather: 1) the high-C/high-S category, which we will call "Strongly Classifiable/Symmetric," had 66 reports; 2) the low-C/low-S category, which we will call "Weakly Classifiable/Asymmetric," with 72 reports; and 3) the moderate-C/low-S category, termed "Moderately Classifiable/Asymmetric," which with 95 reports had the most severe events of any individual category.

Since each of the nine C–S categories were populated by a different number of mesoscale systems, the number of severe weather reports shown for each category in Table 5a was normalized to obtain the average number of severe weather events per MPS (Table 5b). However, the most significant categories for severe weather remain Strongly Classifiable/Symmetric, which produced an average of 16.5 reports per mesoscale precipitation system: Weakly Classifiable/Asymmetric with 12.0, and Moderately Classifiable/Asymmetric with 15.8. Taking a broader view, we see that the average number of severe weather events was about the same for Classifiable mesoscale systems, which averaged 7.3 reports per system, as for Unclassifiable systems, which had an average of 7.7 reports.

The average number of reports per MPS summarized in Table 5b tended to be dominated by a few systems (or "episodes") in which 10 or more severe weather events were reported (see "Total Severe Weather Reports" in column P of Table A1). A total of 17 systems (among the 63 distinct MPSs identified in the radar data) were responsible for such episodes. Thus, roughly one in four systems contributing to major rain events was also associated with a significant outbreak of severe weather. The number of MPSs in each category with ten or more severe weather reports is given in Table 5c. A total of nine of these episodes were associated with Classifiable radar-echo structure, while eight occurred in the presence of Unclassifiable structure. Among the Classifiable systems, the largest number of episodes (4) were associated with Moderately Classifiable/Asymmetric echo structure.

The average numbers of severe weather reports associated with different mesoscale radar-echo structures (Table 5b) were further stratified according to type of severe event in Table 6a–g. Most of the severe weather types exhibited a slight preference for the Classifiable type of organization. For example, the average number of tornadoes per MPS was 1.5 for Classifiable echo structure and 0.9 for Unclassifiable (Table 6a). Hail was the only type of event that exhibited a marked preference for the Unclassifiable type of mesoscale organization, which produced an average of 3.0 reports per MPS compared to just 1.4 for the Classifiable type of organization (Table 6c).

Within Classifiable systems, tornadoes were more common in the low-C categories, where an average of 2.6 tornadoes per mesoscale system were reported, as compared to 1.0 for high-C cases (Table 6a). By contrast, flooding was observed more frequently in the high-C cases, in which 2.4 reports per system were found compared to 0.9 for low-C cases (Table 6f). No other significant trends with respect to C-scores were noted. Tornado occurrence (Table 6a) showed a preference for Asymmetric (low-S) radar-echo organization (3.1 reports per system) as opposed to Symmetric (high-S) organization (0.9 reports per system). Similarly, hail reports (Table 6c) were more common in the Asymmetric systems (2.6 reports per system for the low-S storms, compared to 0.6 for the high-S cases). These results might be anticipated since the Asymmetric systems tend to develop relatively isolated severe cells toward their southern edges, i.e. in regions characterized by greater instability and an absence of nearby cells that might compete for high moist-static energy inflow air or otherwise interfere with their highly or-

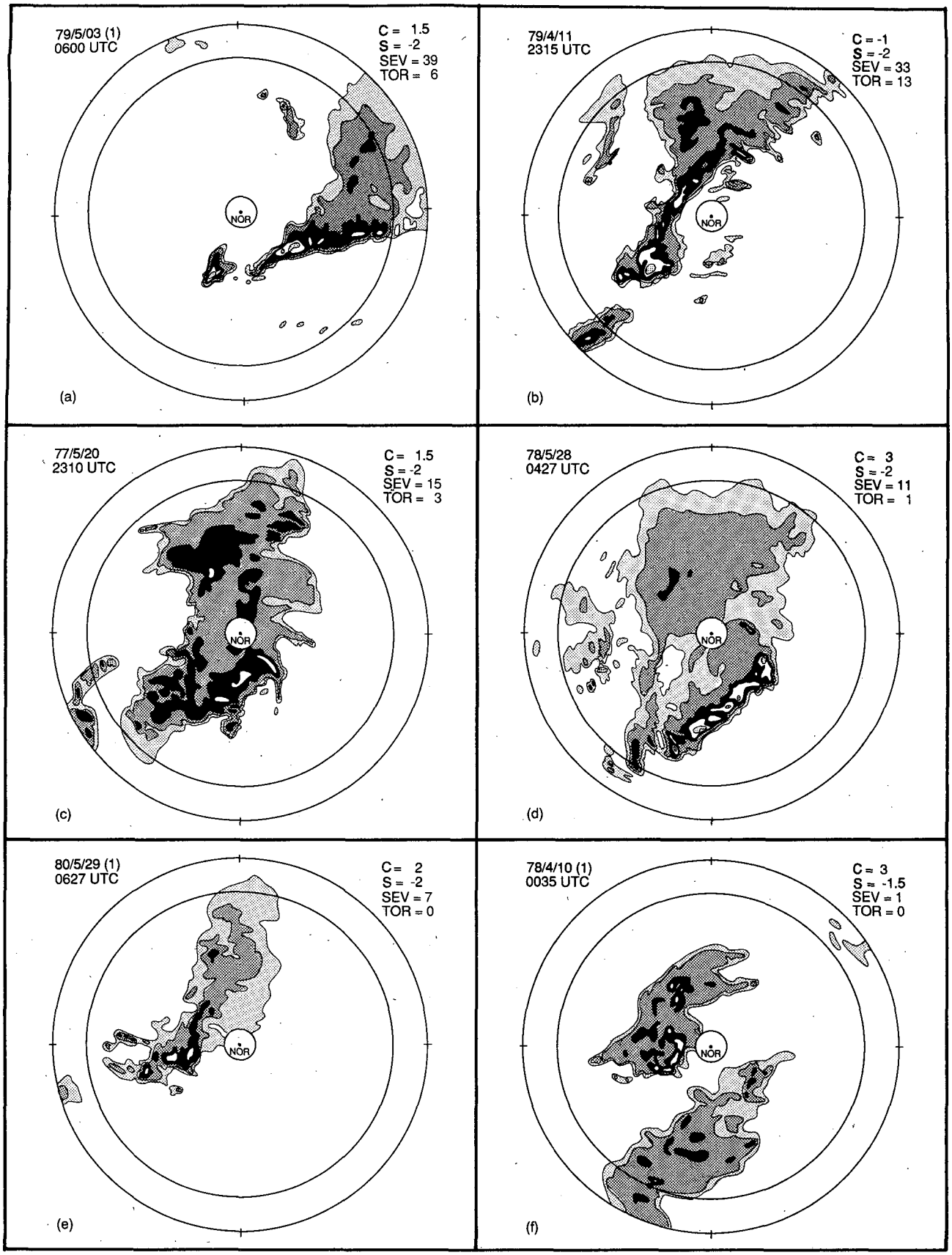

FIG. 13. As in Fig. 9, except for seven examples (a–g) of moderate- and low-C, low-S structure ("Moderately and Weakly Classifiable/Asymmetric"; see text). Total number of severe weather reports and number of tornadoes ("SEV" and "TOR," respectively, from Table 3) reported in study area during passage of system, as well as "C" and "S" scores, are indicated.

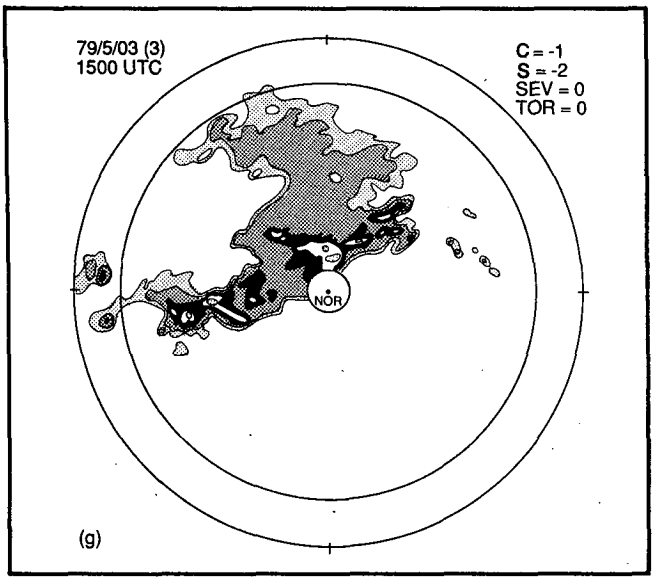

FIG. 13. (*Continued*)

ganized internal circulations. Conversely, flooding reports (Table 6f) were slightly more common in Symmetric systems (2.4 reports per system) as compared to Asymmetric storms (1.9 reports). This result is consistent with the previously noted tendency for flooding to be associated with large stratiform regions, which frequently accompanied Symmetric storms.[3]

c. *Examples of mesoscale radar-echo structure associated with high severe weather occurrence*

According to Table 5, severe weather reports among the Classifiable categories were predominantly associated with the Strongly Classifiable/Symmetric, Moderately Classifiable/Asymmetric and Weakly Classifiable/Asymmetric categories of radar-echo structure, with the Moderately Classifiable/Asymmetric category being the most prolific severe weather producer of all. A large number of severe weather reports also were associated with Unclassifiable radar-echo structure. Examples of Strongly Classifiable/Symmetric and Unclassifiable radar-echo structures were presented in Figs. 9a–b and 10, respectively. These examples help indicate what the radar screen looks like when these types of severe weather episodes take place.

No examples have yet been presented of the Moderately Classifiable/Asymmetric or Weakly Classifiable/Asymmetric organization. It can be argued that these two categories are similar, differing only in degree of resemblance to the leading-line/trailing-stratiform archetype. Taken together, these categories of echo structure represent a very large share of the severe weather occurrence associated with major rain events (Table 5). What do these echo patterns look like? Some systems with Moderately Classifiable/Asymmetric structure are shown in Fig. 13. (Examples of Weakly Classifiable/Asymmetric structure add little insight, and are not shown.)

The examples in Fig. 13 have a strikingly common type of structure, which is characterized by southwest–northeast oriented regions of echo. These regions are narrow at the southwest end, which is intensely convective, while the northeastern part is generally broader and more stratiform. The convection, which tends to be most prevalent in the southwestern portion, occurs in rather discrete, irregularly shaped and arranged cells rather than a highly two-dimensional band. This mode of organization resembles the squall-line systems described by Newton and Fankhauser (1964), shown schematically in Fig. 8. It stands in contrast to the highly classifiable leading-line/trailing-stratiform type of organization (Newton 1950; Fujita 1955; Pedgley 1962; and other studies cited in the Introduction) represented schematically in Fig. 7 and by examples in Fig. 9a and 9b. Thus the interesting result emerges that, when all of the major rain events exhibiting linear structure are examined over a six-year period (i.e., all the major rain events with Classifiable radar-echo structure), the two types of squall lines that attracted attention in early studies (i.e., the Strongly Classifiable/Symmetric "Fujita type" and the Moderately Classifiable/Asymmetric "Newton-Fankhauser type") correspond to the two categories of mesoscale radar-echo structure characterized by the greatest frequency of severe weather.

7. Satellite observations of major rain events

Satellite imagery corresponding to the major rain events listed in Table 2 was examined as described in section 2e. Our primary goal was to determine the extent to which these events were associated with organized mesoscale features identifiable in infrared satellite imagery. Since one particular type of mesoscale cloud organization—the "mesoscale convective complex (MCC)" defined by Maddox (1980)—has received a great deal of attention, we focused on the degree to which major rain events were produced by the passage of MCCs and which (if any) of the types of radar-echo organization identified in section 5 were favored under the cloud shields associated with MCCs. Given the findings of Fritsch et al. (1986) that 30%–70% of the warm-season rainfall over the central United States is associated with such systems, we would expect major

[3] These statistics gauge the frequency of flood reports, but do not take into account their relative severity. It should be noted that severe flash flooding is often associated with radar-echo patterns whose instantaneous structure resembles that of the low-C/low-S (Asymmetric) cases (e.g., Fig. 13.11 of Chappell 1986). However, in contrast to the rapid squall-like movement of the majority of convective lines examined in the present study, such systems are usually quasi-stationary (R. A. Maddox, personal communication).

rain events to be recorded when MCCs pass over Oklahoma.

Of the 19 MCC cloud shields whose centroids are known to have tracked over some portion of the study area during May–June 1978–82, only five failed to produce precipitation sufficient to qualify as a major rain event (according to the definition given in section 2c). It is noteworthy that four of those five MCCs were either in their dissipating stage or only grazed Oklahoma, failing to track more than 50 km into the study area.

We were able to obtain satellite data for 49 of the 55 major rain events listed in Table 2 (data could not be obtained for 1977). Of those 49 events, only 13 (or $\approx$25%) derived all or part of their precipitation from the passage of an MCC (one major rain event, 81/5/29 in Table A1, included contributions from two separate MCCs). Thus, although most of the MCCs were associated with major rain events, a large number of major rain events ($\approx$75%) occurred under cloud shields that failed to meet the MCC criteria. In many cases, however, these cloud shields took on a qualitatively similar appearance akin to MCCs, resembling the "small cloud clusters" described by Bartels et al. (1984).

Not surprisingly, the majority of MCCs that contributed to major rain events developed to the west of the study area (primarily along the Texas–New Mexico border and extending northward to the border between southeast Colorado and southwest Kansas) and tracked with an eastward component. A few of these satellite-observed cloud shields developed either north or south of the study area and subsequently expanded into it.

As established in previous sections, a given major rain event was sometimes associated with the passage of more than one mesoscale precipitation system identified on radar. Thus, a somewhat more precise way of examining the data is to consider the individual MPSs (listed in Table A1) which contributed to the major rain events (Table 2). The satellite and radar data were carefully compared to determine which of the individual precipitation systems were associated with MCCs. Particular attention was given to the types of mesoscale radar-echo organization exhibited by these systems. The results of this comparison are presented in Table 7, which allows us to infer the relationship between mesoscale radar-echo organization and MCC-type cloud shield structure. The numbers in the table are given as ratios where the numerator is the number of MPSs found to occur beneath an MCC cloud shields, while the denominator is the total number of MPSs in that category for which satellite data were available. In several cases, multiple MPSs were observed beneath a single MCC cloud shield.

The data in Table 7 indicate no strong tendency for any one type of radar-echo structure to be preferred in MCCs. Altogether, 16 of 55 (or $\approx$30%) of all the mesoscale systems described by satellite data occurred in association with MCC cloud structure. Nine out of 35 (or $\approx$25%) of the systems exhibiting Classifiable echo structure developed beneath MCC cloud shields, while a slightly greater fraction (7 out of 20, or $\approx$35%) of Unclassifiable systems were associated with MCCs. This difference is not judged to be significant, however. Within the classifiable categories, no obvious preference for attainment of MCC cloud shield characteristics with respect to parameters C or S is indicated.

8. Environmental conditions associated with major rain events

a. Methodology

In sections 4 and 5 it was demonstrated that although the precipitation patterns associated with major rain events exhibit a diverse spectrum of mesoscale organization, certain recognizable mesoscale structures tend to recur. Moreover, in section 6 it was shown that several of these structures are associated with a particularly high frequency of severe weather. These results give rise to the question: Can the environments supporting dissimilar types of mesoscale structure be differentiated using standard sounding data?

Following an approach analogous to that employed by Bluestein and Jain (1985), soundings pertaining to the 42 Classifiable MPSs and 21 Unclassifiable MPSs

TABLE 7. Ratio of mesoscale precipitation systems (MPSs) occurring beneath cloud shields qualifying as mesoscale convective complexes (numerator) to total number of MPSs in each category of mesoscale radar echo organization (denominator).

		Type of organization			
Degree of organization	Range of scores	Symmetric $S \geq 1$	Intermediate $-1 < S < 1$	Asymmetric $S \leq -1$	All types All S
Strongly Classifiable	$C > 5$	2/4	0/4	0/3	2/11
Moderately Classifiable	$0 \leq C \leq 5$	0/4	2/6	2/5	4/15
Weakly Classifiable	$C < 0$	1/1	1/3	1/5	3/9
All Classifiable systems	All C	3/9	3/13	3/13	9/35
All Unclassifiable systems					7/20

listed in Table A1 were gathered and analyzed. It should be emphasized that, in contrast to the near-environment picture constructed by Bluestein and Jain (who made use of special soundings taken immediately ahead of squall lines), our analysis is based upon the standard synoptic soundings from Oklahoma City, located near the center of the study area, at 0000 and 1200 UTC daily. The soundings considered were taken an average of 5 h (≈250 km) ahead of storms that crossed the study area, although release times ranged from less than an hour to as long as 11 h prior to storm passage. Subject to the considerations described in section 2f, representative soundings (one per system) were obtained for 45 out of 63 (≈70%) of the systems listed in Table A1. Groups of soundings were assembled for storms exhibiting similar mesoscale structure (as will be described in section 8b) and mean sounding profiles, and hodographs and averages of derived parameters were calculated (sections 8c–d). Differences between derived sounding parameters for various groups were evaluated and subjected to tests for statistical significance to identify their relationship to the type and degree of mesoscale storm organization (section 8e–h).

Detailed case studies of convectively-driven precipitation systems often reveal considerable mesoscale spatial and temporal variations of atmospheric conditions in the vicinity of these storms. Unfortunately, the special datasets required to address such variations were rarely collected over the study area. While they are by no means a substitute for actual mesoscale measurements, the Oklahoma City soundings have the advantage of being available for the entire six-year study period. Some increased variance (and commensurate reduction of statistical significance) of parameters sampled in this gross manner likely results from differences in sounding location and release time with respect to the complex and evolving environments of such storms. This limitation is shared by current forecast techniques making use of standard synoptic data, and is central to the mesoscale forecast problem.

b. Groupings of soundings for the 1977–82 study period

To obtain larger sample sizes suitable for statistical analysis, we departed from the system of nine basic categories (defined in terms of the parameters C, measuring the degree of resemblance to the leading convective/trailing-stratiform archetype, and S, which measures resemblance to the Symmetric or Asymmetric type of organization) described in section 5. Rather, an analogous subdivision based upon these same parameters but containing only six categories was made as follows:

Category 1: $C > 5$ and $S \geq 0$ "Strongly Classifiable and Symmetric."

Category 2: $0 \leq C \leq 5$ and $S \geq 0$ "Moderately Classifiable and Symmetric."

Category 3: $C < 0$ and $S \geq 0$ "Weakly Classifiable and Symmetric."

Category 4: $C > 5$ and $S < 0$ "Strongly Classifiable and Asymmetric."

Category 5: $0 \leq C \leq 5$ and $S < 0$ "Moderately Classifiable and Asymmetric."

Category 6: $C < 0$ and $S < 0$ "Weakly Classifiable and Asymmetric."

Additionally, two categories were defined for systems displaying Unclassifiable structure; for reasons that will become apparent, the Unclassifiable systems were subdivided according to the number of severe weather events reported:

Category 7: Unclassifiable with ≥10 severe weather reports, "Unclassifiable/Severe."

Category 8: Unclassifiable with <10 severe weather reports, "Unclassifiable/Nonsevere."

Mean soundings and hodographs were constructed for each of these eight categories. They are not all shown here (although a comprehensive list of derived parameters is given in Table 8). Instead, we focus on mean soundings for particularly illuminating combinations of the basic categories. First, mean conditions for all of the major rain events (without regard to the type of radar-echo organization, obtained by considering all 45 soundings in Categories 1–8) are shown in Fig. 14. To illustrate conditions associated with Classifiable radar-echo structure, the average sounding for all the Classifiable systems (Categories 1–6 combined) is shown in Fig 15. Then three subgroups—formed by combining Categories 1 and 4, 2 and 5, and 3 and 6—serve to contrast the environments of systems that displayed, respectively, strong, moderate, and weak degrees of leading-line/trailing-stratiform structure (Figs. 16–18). The mean environment of all Unclassifiable MPSs (Categories 7 and 8 combined) is shown in Fig. 19. The soundings for Categories 7 and 8 are shown separately in Figs. 20 and 21 to differentiate the conditions supporting Unclassifiable/Severe and Unclassifiable/Nonsevere mesoscale structure. In order to distinguish the environments of the Symmetric and Asymmetric forms of leading-line/trailing-stratiform precipitation structure, soundings for Categories 1+2+3 and 4+5+6 are shown in Figs. 22 and 23, respectively.

To quantify differences in environments supporting diverse modes of mesoscale organization, mean values of familiar parameters were calculated for the eight individual categories and their various combinations, and are listed in Tables 8 and 9. These values were computed for individual soundings in each group (not from the mean sounding profiles) and then averaged; differences and trends in meteorological conditions corresponding to contrasting modes of mesoscale organization were noted. To evaluate the significance of these sampled differences, the Student's t-test was applied to various pairs of groupings indicated by brackets in Tables 8 and 9; confidence levels associated with differences so obtained are also indicated.

TABLE 8. Mean derived parameters (Rows 4–25) and number of soundings used (Row 26) for individual categories 1–8 (Columns D–K, respectively) of mesoscale radar-echo organization (see text). Brackets indicate pairs of categories whose differences were tested for statistical significance. Confidence levels (%) for differences in parameter values that were noteworthy in a statistical sense are indicated in the rightmost member of each bracketed pair according to the following key: ✓ ✓ ✓ ✓ ✓, ≥99%; ✓ ✓ ✓ ✓, ≥98%; ✓ ✓ ✓, ≥97.5%; ✓ ✓, 95%; ✓, ≥90%; ✓−, ≥80%; ✓−−, ≥75%.

	A	B	C	D	E	F	G	H	I	J	K
1				Category 1	Category 2	Category 3	Category 4	Category 5	Category 6	Category 7	Category 8
2				Strongly Clsfbl	Moderately Clsfbl	Weakly Clsfbl	Strongly Clsfbl	Moderately Clsfbl	Weakly Clsfbl	Unclassifiable w/	Unclassifiable w/
3				and Symmetric	and Symmetric	and Symmetric	and Asymmetric	and Asymmetric	and Asymmetric	≥ 10 Severe Rpts	< 10 Severe Rpts
4	Vector-mean Wind 3-10 km [Dir°/Speed (m/s)]			234/13.7	238/14.9	268/18.8	236/15.2	239/16.2	234/20.8	264/17.3 ✓	243/14.6
5	Vertical Shear Sfc-2.5 km [Dir°/Speed(m/s)]			237/6.8	256/7.7	277/9.5	264/9.1	254/9.3	204/14.8	251/11.6 ✓−−	255/9.4
6	Vertical Shear 2.5 - 6 km [Dir°/Speed(m/s)]			289/8.3	253/7.4	268/11.1	223/7.5	253/7.5	274/11.3	267/8.9 ✓	271/5.3
7	Vertical Shear Sfc-6.0 km [Dir°/Speed(m/s)]			266/13.5	255/15.1	272/20.6	246/15.5	254/16.7	234/21.6	266/19.5 ✓	261/14.6
8	Freezing Level (mb/km agl)			605/3.9	641/3.4	609/3.9	627/3.6	619/3.7	620/3.7	625/3.7	629/3.6
9	Wet-Bulb Zero Level (mb/km agl)			660/3.2	653/3.3	711/2.6	664/3.2	678/3.0	640/3.4	691/2.9	675/3.0
10	Lifted Index (°C)			-4.7	-3.5	-3.5	-4	-5.2	-0.8	-3.7	-3.7
11	Totals-Totals Index (°C)			51.2	51.7	55.3	49.4	53.6	50.3	53.3	51.7
12	K-Index (°C)			29	34.9	29.2	32.8	28.4	36	34.3 ✓−	28.6
13	Precipitable Water (cm)			3.4	3.4	3.2	3.7	3.3	3.7	3.2	3.2
14	Lifting Condensation Level (mb/km agl)			860/1.4	864/1.3	885/1.2	877/1.2	875/1.2	873/1.3	821/1.8 ✓✓✓✓	885/1.1
15	Level of Free Convection (mb/km agl)			731/2.8	728/2.8	598/4.4	763/2.4	741/2.7	789/2.2	714/3.0	726/3.0
16	Equilibrium Level (mb/km agl)			215/11.9	309/9.6	258/10.5	243/11.0	215/11.8	394/8.9	277/10.4	257/9.6
17	Convective Temperature (°C)			30.1	28.1	28.7	26	27.6	25.9	30.8 ✓−	25.7
18	Maximum Updraft Velocity (m/s)			35.7	27.8	19.1	31.1	39.6	21.8	30.6	28.8
19	Convective Available Potential Energy ('CAPE', J/kg)			1497	941	510	1037	1632	718	1095	1109
20	Convective Inhibition ('CIN', J/kg)			-72	-113	-236	-39	-87	-66	-98	-132
21	Bulk Richardson Number			116.3	34.5	10.6	28	65.2	10.7	25	18.5
22	Boundary Layer Parcel Temperature (°C)			23.4	21.2	19.8	22	21.9	20	24.1 ✓✓	20
23	Boundary Layer Parcel Mixing Ratio (g/kg)			13.7	12.4	12.2	13.4	13.3	11.9	11.8	12.8
24	Boundary Layer Parcel Dew Point (°C)			17.5	15.8	15.8	17.4	17.2	15.1	14.9	16.3
25	Boundary Layer Parcel Dew Point Depression (°C)			5.9	5.4	4	4.6	4.7	4.9	9.2	3.7
26	Number of Soundings in Category			8	6	2	3	7	4	7	8

In section 8c, we describe briefly the general characteristics of the mean soundings, both for all cases combined (i.e., regardless of MPS structure) and for the major subgroups. Then in subsections d–h, we make a number of comparisons between selected pairs of subgroups. These comparisons are the primary method by which we attempt to distinguish the environments associated with contrasting modes of mesoscale organization.

c. *Mean soundings and hodographs*

1) ALL MAJOR RAIN EVENTS

Several general characteristics of the environments of major rain events in Oklahoma are summarized by the mean thermodynamic profile and hodograph comprising all of the soundings used in the analysis (Fig. 14), as well as in Column D of Table 9. The mean thermodynamic stratification is conditionally unstable through much of the troposphere. A stable layer is indicated near 800 mb, evidence of low-level capping at the top of the boundary layer. Owing to effects of averaging soundings with varying boundary-layer depths, this feature (which often takes the form of a sharp inversion) has been smoothed appreciably. Nonetheless, its appearance in the mean sounding speaks for its frequent presence in association with major springtime rain events over Oklahoma. The thermodynamic profile reflects generally well-mixed conditions below the stable layer; lapse rates approached dry-adiabatic in some cases. Conditionally unstable conditions are evident from the top of the stable layer to the tropopause, which lay near 200 mb in the mean.

Mean winds exhibit a structure commonly associated with Oklahoma thunderstorms, with southerly boundary-layer flow sharply veering to become southwesterly through the remainder of the troposphere. Hodograph curvature below 700 mb is principally related to the presence of a low-level southerly jet, a feature indigenous to the southern plains of the United States (e.g., Bonner 1968). Although the low-level jet appears in this mean sounding, it is not a ubiquitous feature for the cases examined: while it is a prominent characteristic of some of the types of mesoscale organization, it is weak or nonexistent in other categories (as will be discussed). Above the jet the mean shear tends to become more unidirectional, with westerly winds increasing to a maximum of 26 m s^{-1} just above 200 mb and falling off sharply thereafter in the lower stratosphere.

2) SYSTEMS DISPLAYING "CLASSIFIABLE" MESOSCALE RADAR-ECHO STRUCTURE

The mean sounding for "Classifiable" storms—those embodying some degree of leading-line/trailing-stratiform structure—is shown in Fig. 15. In general, it resembles the average sounding for all systems shown in Fig. 14. The features of the Classifiable cases are perhaps best seen by examining the trends moving from Strongly to Weakly Classifiable systems (Figs. 16–18). The height of the stable layer (related to the low-level inversion seen in individual soundings) decreases as one moves toward less classifiable systems (i.e., lower values of C). In addition, less classifiable storms (represented by Weakly Classifiable systems in Fig. 18) are associated with all of the following: cooler, more stable boundary-layer conditions; minimal hodograph curvature, with little sign of the low-level jet seen in the hodograph for the Strongly Classifiable systems (cf. Fig.

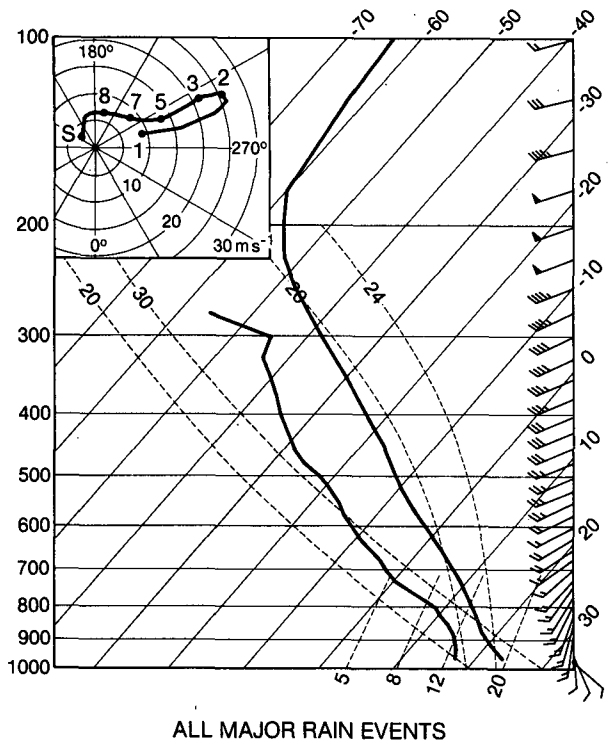

FIG. 14. Mean sounding and hodograph for all Mesoscale Precipitation Systems occurring during Major Rain Events (defined in text). Temperature and dewpoint curves (°C) are shown by heavy lines. Ground-relative winds are plotted on vertical (pressure, mb) axis according to the convention: half barb, 2.5 m s^{-1}; full barb, 5 m s^{-1}; flag, 25 m s^{-1}. Dry adiabats (labeled 20° and 30°C), moist adiabats (labeled 20° and 24°C) and lines of constant saturation mixing ratio (5, 8, 12 and 20 g kg^{-1}) are shown for reference. In hodograph (inset) rings are at 5 m s^{-1} intervals and wind profile is indicated by heavy curve; points along curve labeled "S," "8," "7," "5," "3," "2," and "1," denote surface, 850 mb, 700 mb, 500 mb, 300 mb, 200 mb, and 100 mb levels, respectively.

16); and appreciably greater vertical wind shear at low- to mid-levels.

3) SYSTEMS WITH "UNCLASSIFIABLE" RADAR-ECHO STRUCTURE

The mean sounding for all "Unclassifiable" systems (Categories 7+8) is shown in Fig. 19. The environmental characteristics of these storms are better seen, however, by decomposing the sample based on storm severity. The mean sounding for the Unclassifiable/Severe systems (Category 7, Fig. 20), which included a number of cases marked by the occurrence of scattered supercell-like storms, is characterized by a very unstable boundary layer and has other attributes classically found in severe weather environments (e.g., Fawbush and Miller 1954). By contrast, the less severe Unclassifiable storms (Category 8, Fig. 21) occurred in the presence of generally more stable stratifications—especially in the boundary layer—and weaker vertical wind shear.

d. Comparison of environments supporting Strongly, Moderately and Weakly Classifiable radar-echo structure

1) PROCEDURE

It was found in section 5 that leading-line/trailing-stratiform structure, which we have termed "Classifiable" structure, occurs in degrees ranging from Strongly through Moderately, to Weakly Classifiable (e.g., top three rows of Table 3). In this section, we investigate whether corresponding differences in the environment can be seen as the degree of leading-line/trailing-stratiform structure varies from Strongly to Weakly Classifiable. The soundings for these three groupings are shown in Figs. 16–18. Derived sounding parameters for these groups are listed in Table 9, and trends in their values corresponding to progression from Strongly to Moderately to Weakly Classifiable environments may be examined by moving from left to right across columns E–G. The statistical confidence levels (shown symbolically in column G) indicate those parameters that emerge as being most important in serving to differentiate the environments of Strongly and Weakly Classifiable systems. Basic differences in the wind shear

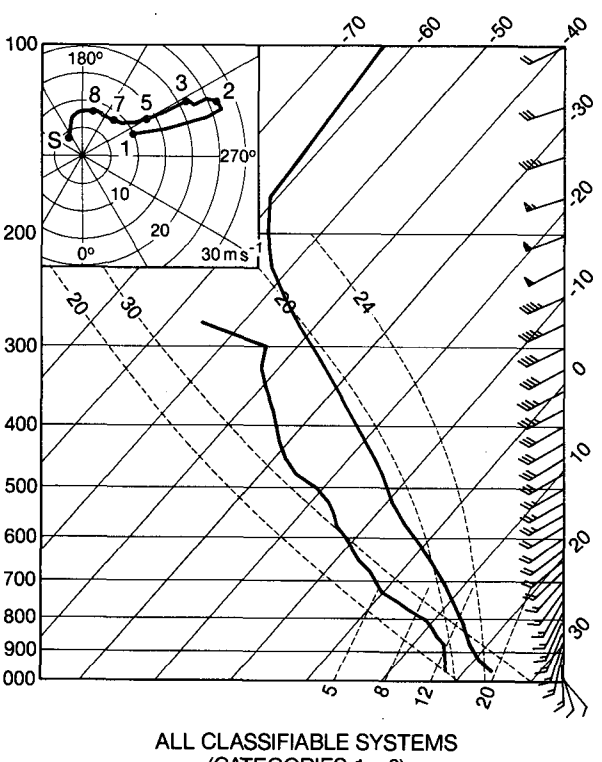

FIG. 15. As in Fig. 14 except for all Classifiable systems (Categories 1–6).

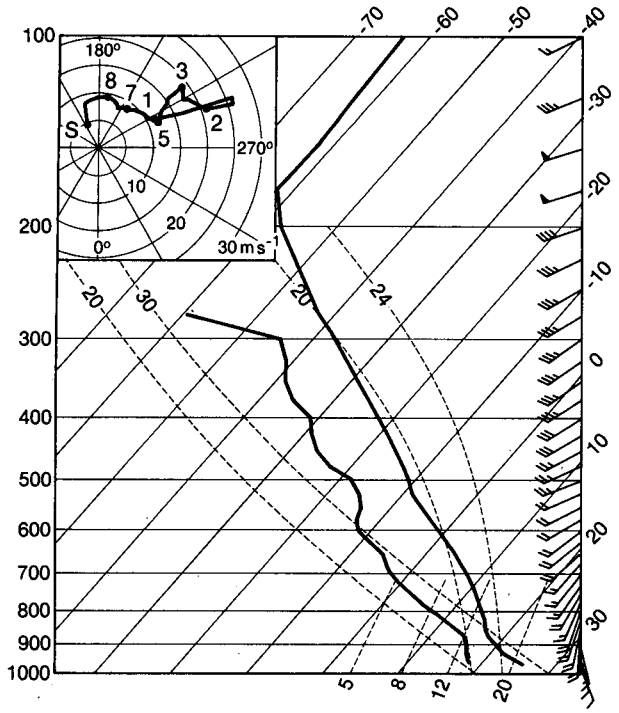

STRONGLY CLASSIFIABLE SYSTEMS
(CATEGORIES 1 AND 4)

FIG. 16. As in Fig. 14 except for Strongly Classifiable systems (Categories 1 and 4).

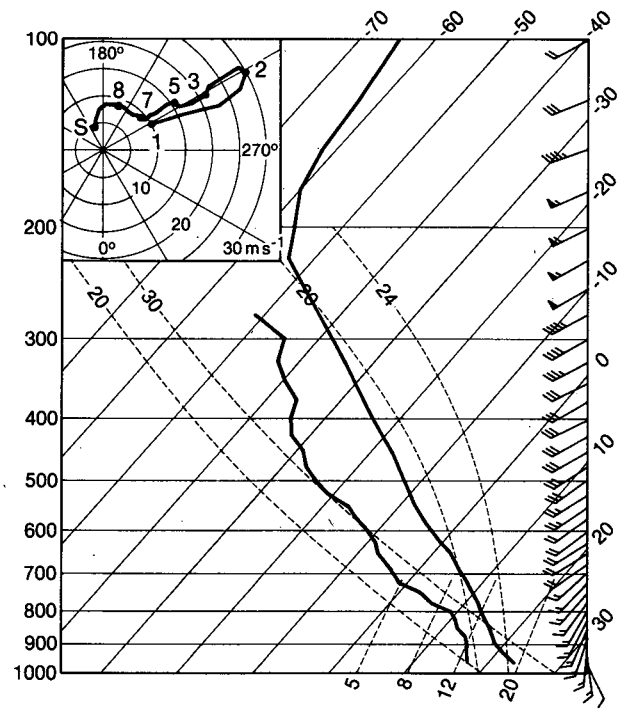

MODERATELY CLASSIFIABLE SYSTEMS
(CATEGORIES 2 AND 5)

FIG. 17. As in Fig. 14 except for Moderately Classifiable systems (Categories 2 and 5).

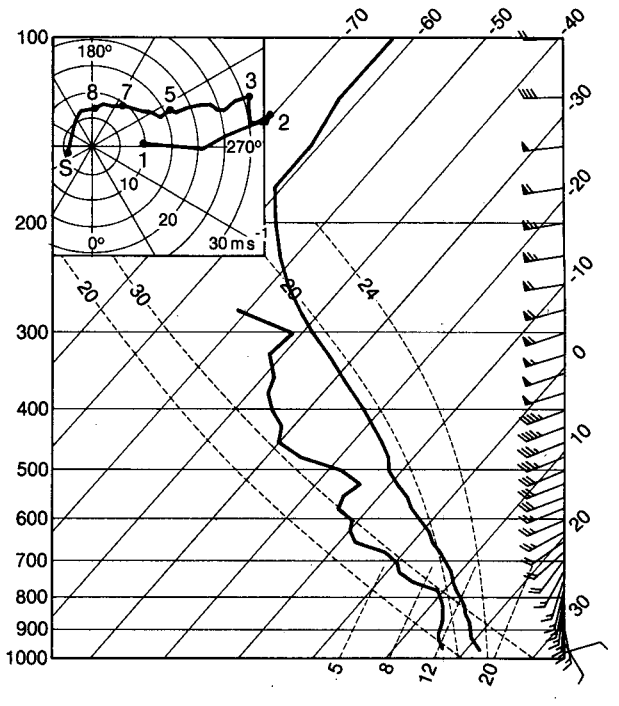

WEAKLY CLASSIFIABLE SYSTEMS
(CATEGORIES 3 AND 6)

FIG. 18. As in Fig. 14 except for Weakly Classifiable systems (Categories 3 and 6).

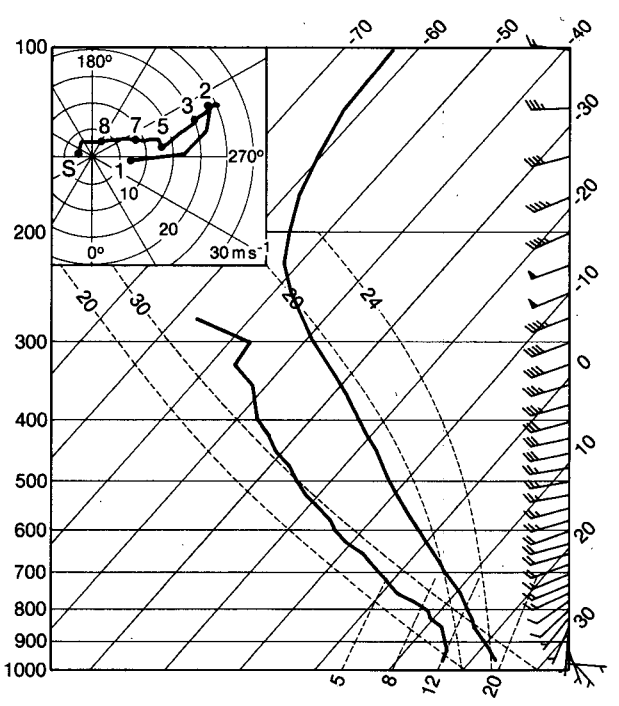

ALL UNCLASSIFIABLE SYSTEMS
(CATEGORIES 7 AND 8)

FIG. 19. As in Fig. 14 except for all Unclassifiable systems (Categories 7 and 8).

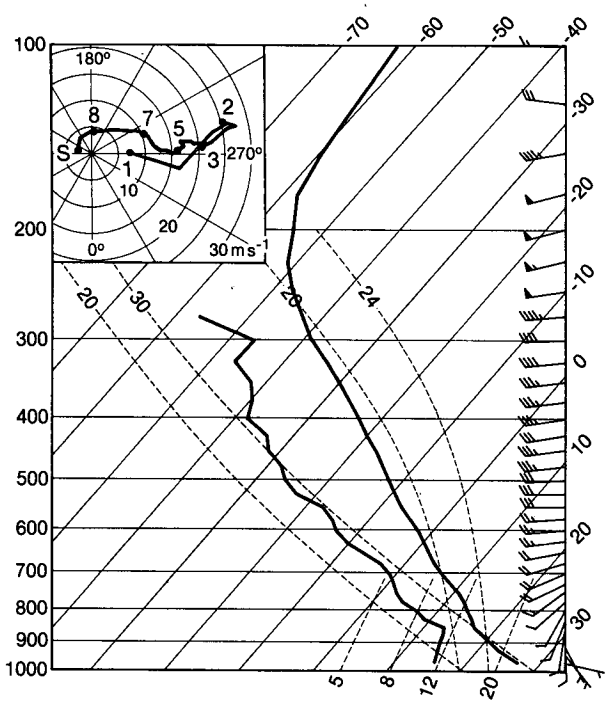

FIG. 20. As in Fig. 14 except for Unclassifiable/Severe systems, i.e. those with ≥10 severe weather reports (Category 7).

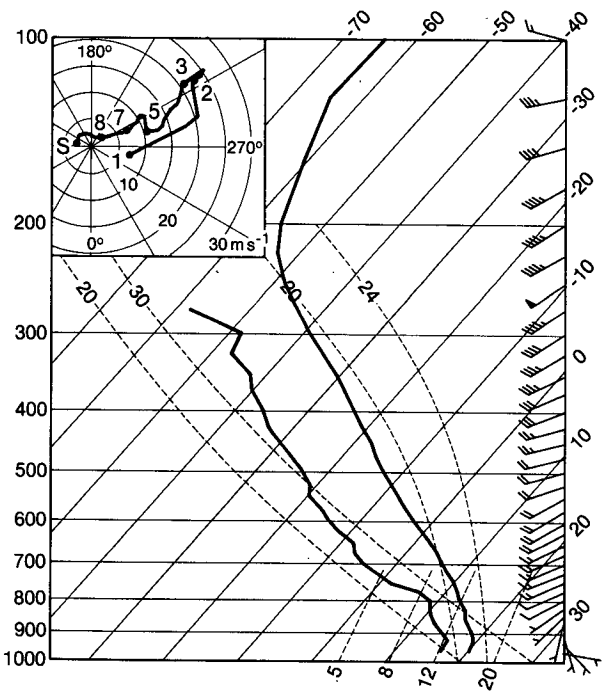

FIG. 21. As in Fig. 14 except for Unclassifiable/Nonsevere systems, i.e. those with <10 severe weather reports (Category 8).

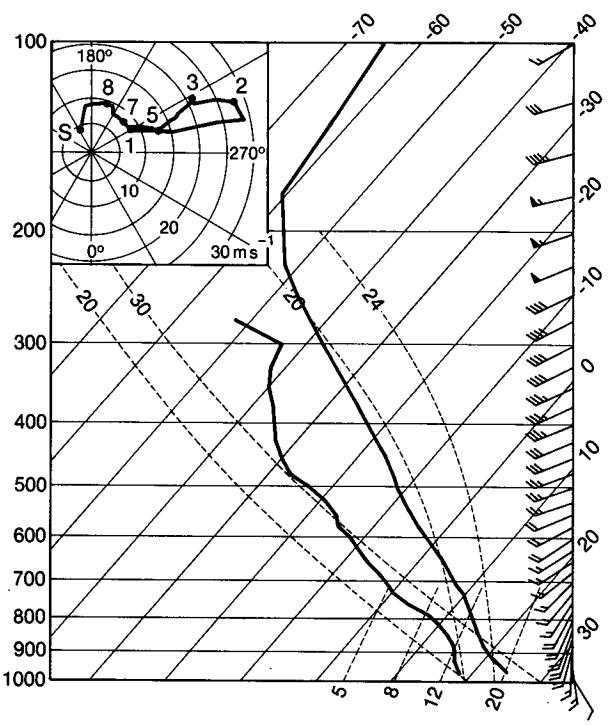

FIG. 22. As in Fig. 14 except for all Symmetric systems (Categories 1, 2 and 3).

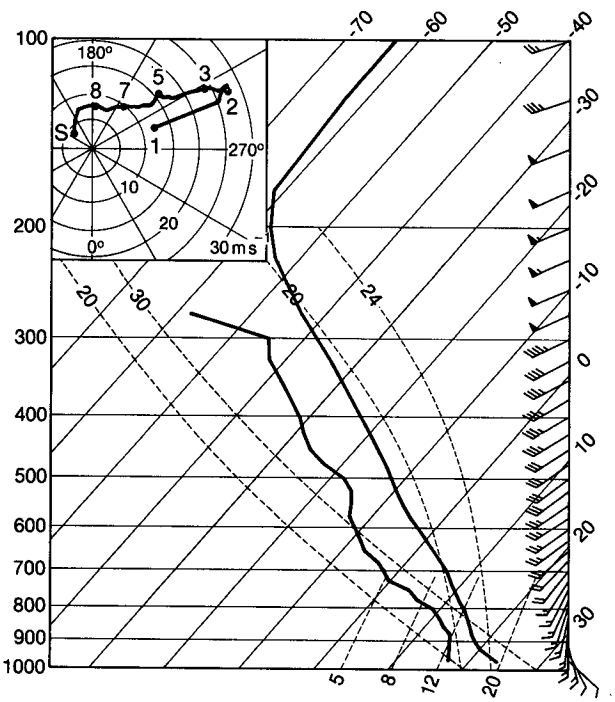

FIG. 23. As in Fig. 14 except for all Asymmetric systems (Categories 4, 5 and 6).

TABLE 9. As in Table 8, except for various combinations of individual categories (see text).

Table 9—Part I

	A	B	C	D	E	F	G	H
1				All Categories (1-8)	Categories 1+4	Categories 2+5	Categories 3+6	Categories 7+8
2				All MPSs During	Strongly	Moderately	Weakly	All Unclassifiable
3				Major Rain Events	Classifiable Cases	Classifiable Cases	Classifiable Cases	Cases
4	Vector-mean Wind 3-10 km [Dir°/Speed (m/s)]			244/15.7	235/14.1	239/15.6	√√ 244/19.4	√ 254/15.6
5	Vertical Shear Sfc-2.5 km [Dir°/Speed(m/s)]			247/9.0	246/7.2	255/8.5	√− 220/11.3	√ 253/10.4
6	Vertical Shear 2.5 - 6 km [Dir°/Speed(m/s)]			270/7.6	274/7.1	253/7.4	√√ 272/11.2	280/6.9
7	Vertical Shear Sfc-6.0 km [Dir°/Speed(m/s)]			257/16.2	260/13.9	254/16.0	√− 246/20.2	√− 264/16.9
8	Freezing Level (mb/km agl)			622/3.7	611/3.8	629/3.6	617/3.8	√−− 627/3.6
9	Wet-Bulb Zero Level (mb/km agl)			670/3.1	661/3.2	666/3.1	664/3.2	√− 683/2.9
10	Lifted Index (°C)			-3.8	-4.5	-4.4	√− -1.7	-3.7
11	Totals-Totals Index (°C)			52	50.7	52.7	52	52.5
12	K-Index (°C)			31.3	30	31.4	√−− 33.7	31.2
13	Precipitable Water (cm)			3.4	3.5	3.3	3.5	√− 3.2
14	Lifting Condensation Level (mb/km agl)			865/1.3	865/1.4	870/1.3	√− 877/1.2	√− 856/1.4
15	Level of Free Convection (mb/km agl)			730/2.9	740/2.7	735/2.7	725/3.0	720/3.0
16	Equilibrium Level (mb/km agl)			265/10.5	223/11.6	258/10.8	√− 349/9.4	√− 267/10.0
17	Convective Temperature (°C)			28.1	29	27.8	26.8	28.1
18	Maximum Updraft Velocity (m/s)			31	34.5	34.1	√ 20.9	29.7
19	Convective Available Potential Energy ('CAPE', J/kg)			1169	1372	1313	√−− 649	1102
20	Convective Inhibition ('CIN', J/kg)			-98	-63	-99	√−− -123	√− -115
21	Bulk Richardson Number			44.3	89.8	51	√−− 10.7	√− 21.5
22	Boundary Layer Parcel Temperature (°C)			21.8	23	21.6	√− 20	21.9
23	Boundary Layer Parcel Mixing Ratio (g/kg)			12.7	13.6	12.9	√− 11.9	√−− 12.3
24	Boundary Layer Parcel Dew Point (°C)			16.3	17.5	16.5	√− 15.3	√− 15.7
25	Boundary Layer Parcel Dew Point Depression (°C)			5.5	5.5	5.1	√− 4.7	6.2
26	Number of Soundings in Category			45	11	13	6	15

Table 9—Part II

	A	B	C	H	I	J	K	L	M
1				Categories 7+8	Categories1+2+3	Categories4+5+6	Categories 1-6	Categories 1+2	Categories 5+6
2				All Unclassifiable	All Symmetric	All Asymmetric	All Classifiable	Stgly&Mod Classifbl	Mod&Wkly Classifbl
3				Cases	Cases	Cases	Cases	Symmetric Cases	Asymmetric Cases
4	Vector-mean Wind 3-10 km [Dir°/Speed (m/s)]			254/15.6	241/14.6	√−− 237/17.3	√ 239/15.9	236/14.3	237/17.9
5	Vertical Shear Sfc-2.5 km [Dir°/Speed(m/s)]			253/10.4	251/7.2	√− 237/9.7	√− 243/8.3	246/7.1	231/10.2
6	Vertical Shear 2.5 - 6 km [Dir°/Speed(m/s)]			280/6.9	274/8.0	256/8.1	√−− 265/7.9	275/7.5	263/8.7
7	Vertical Shear Sfc-6.0 km [Dir°/Speed(m/s)]			264/16.9	263/14.9	√ 245/17.6	√−− 254/16.0	261/14.1	245/18.2
8	Freezing Level (mb/km agl)			627/3.6	619/3.7	621/3.7	620/3.7	620/3.7	620/3.7
9	Wet-Bulb Zero Level (mb/km agl)			683/2.9	664/3.2	664/3.2	√ 664/3.2	657/3.2	664/3.2
10	Lifted Index (°C)			-3.7	-4.1	-3.7	-3.9	-4.1	-3.6
11	Totals-Totals Index (°C)			52.5	51.9	51.7	51.8	51.4	52.4
12	K-Index (°C)			31.2	31.2	31.5	31.4	31.5	31.2
13	Precipitable Water (cm)			3.2	3.4	3.5	3.4	3.4	3.5
14	Lifting Condensation Level (mb/km agl)			856/1.4	865/1.3	875/1.3	868/1.3	862/1.4	874/1.3
15	Level of Free Convection (mb/km agl)			720/3.0	713/3.0	√−− 759/2.5	√−− 735/2.8	730/2.8	758/2.5
16	Equilibrium Level (mb/km agl)			267/10.0	256/10.9	272/10.8	263/10.8	256/10.9	280/10.7
17	Convective Temperature (°C)			28.1	29.2	26.8	√−− 28.1	29.3	27
18	Maximum Updraft Velocity (m/s)			29.7	30.7	32.7	31.6	32.3	33.1
19	Convective Available Potential Energy ('CAPE', J/kg)			1102	1165	1243	1202	1259	1300
20	Convective Inhibition ('CIN', J/kg)			-115	-108	-71	-90	-89	-79
21	Bulk Richardson Number			21.5	69.5	41.6	√−− 56	78.5	45.4
22	Boundary Layer Parcel Temperature (°C)			21.9	22.1	21.4	21.8	22.5	21.2
23	Boundary Layer Parcel Mixing Ratio (g/kg)			12.3	13	12.9	13	13.1	12.8
24	Boundary Layer Parcel Dew Point (°C)			15.7	16.6	16.6	16.6	16.8	16.4
25	Boundary Layer Parcel Dew Point Depression (°C)			6.2	5.9	4.8	5.2	5.7	4.8
26	Number of Soundings in Category			15	16	14	30	14	11

accompanying Strongly and Weakly Classifiable systems are further summarized graphically in Figs. 24a and 24b.

2) WIND PROFILES

We begin by considering various attributes of the wind profiles (rows 4–7 of Table 9). Strongly Classifiable systems tend to be associated with moderate southwesterly winds in the 3–10 km layer; the mean wind veers and strengthens as the degree of "classifiability" decreases. Application of the Student's t-test shows this difference between environments of Strongly versus Weakly Classifiable MPSs to be significant at the 95% level.

Important differences are also indicated for the vertical wind shear. The strength and depth of shear also grow with decreasing degree of resemblance to the leading-line/trailing-stratiform archetype. The magnitudes of both the low-level (0–2.5 km) and mid-level (2.5–6 km) shear increase monotonically as one progresses from Strongly to Weakly Classifiable storms. These increases are significant at the 80% and 95% levels, respectively. Another manifestation of this contrast is evident from comparison of hodographs for these groups (Figs. 16–18). Only slight hodograph curvature is evident below 500 mb in the environments of Weakly Classifiable storms (Fig. 18), while a marked southerly low-level jet results in strong hodograph curvature

around the 850 mb level in association with Strongly Classifiable systems (Fig. 16).

Although summary graphs of the mean vertical wind shear for Strongly and Weakly Classifiable systems (Figs. 24a and 24b) smooth out some important details, such as the low-level jet in the Strongly Classifiable category, they readily illustrate the general character of the shear ahead of these diverse mesoscale systems. The mean southwest–northeast orientation observed for lines moving across the study area is also indicated in the graphs.[4] From Fig. 24a, the Strongly Classifiable systems are seen to have occurred in the presence of relatively weak shear in both the low and low-to-mid troposphere, as already noted. By contrast, Weakly Classifiable systems were associated with appreciably stronger shear at both low and middle levels (Fig. 24b).

Although the overall shear is stronger in the Weakly Classifiable systems than in the Strongly Classifiable ones, the component of shear normal to the line in the lowest 6 km is similar ($\approx$9 m s^{-1}). This result can be interpreted in view of recent numerical studies. Rotunno et al. (1988) and Weisman et al. (1988) (collectively referred to as RWK) focused on the relationship of squall-line structure and evolution to the line-normal vertical wind shear. They found that squall lines developing in environments with weak line-normal shear evolve toward an "upshear-tilted" state in which rapidly regenerating, short-lived cells occupy a relatively wide leading band and preferentially detrain moisture and momentum rearward into the zone where our observations frequently indicate a broad trailing region of lighter stratiform rain. A generally similar dependence of squall-line structure on shear was found by Fovell and Ogura (1988, 1989), who demonstrated further that systems may persist in the upshear-tilted state for long periods of time.

Evidently, Strongly and Weakly Classifiable systems are similar in the respect that they have line-normal shear of sufficient magnitude to support a long-lived line that develops upshear tilt and a trailing-stratiform region. The salient difference between the environments supporting these contrasting storm types apparently rests in the magnitude of the *along-line* component of the shear. The "classifiability" of the line relates to the degree to which the leading line of convection displays the characteristics indicated in Figs. 7 and 8, i.e. arc shape, solid appearance, etc. The weaker overall shear in the case of the Strongly Classifiable lines apparently favors these characteristics. One notable characteristic of Strongly Classifiable squall systems is that they exhibit organized-multicellular structure in the cross-line direction along their entire length (e.g., Smull and Houze 1985, 1987a,b; Rutledge et al. 1988). Development of organized-multicellular convective structure is consistent with weaker shear, as will be discussed further in section 8d(4). Conversely, we speculate that the stronger shear accompanying Weakly Classifiable cases favors supercellular structure for some elements in their convective lines. Such structure would be consistent with the more frequent occurrence of tornadoes in this category of mesoscale organization (Table 6a). Because of the intensity and three-dimensionality of supercell air motions, their presence along the convective line would be expected to disrupt the structure of the line, lending it a more irregular (i.e., less classifiable) structure.

3) THERMODYNAMIC PROFILES

Additional distinctions between the environments of Strongly and Weakly Classifiable systems are suggested by comparison of derived thermodynamic parameters, but are significant only at the 80% level. While these findings are supported by consistent trends across all three categories (Columns E–G of Table 9), they must be viewed with caution. Environments of Weakly Classifiable systems are generally more stable than those of Strongly Classifiable ones (exhibiting a Lifted Index that is higher by an average of 2.8°C). They exhibit a slightly lower (by 0.2 km) lifting-condensation level and appreciably lower (by 2.2 km) equilibrium level. Weakly Classifiable systems are also associated with greater convective inhibition[5] (by 60 J kg^{-1}) and cooler temperatures in the lowest 500 m (by 3°C). This trend was previously noted in Figs. 16–18 (section 8c). Although the absolute amount of moisture (as measured by the water vapor mixing ratio) was less for Weakly Classifiable systems, owing to the much cooler temperatures the relative humidity at low levels was actually greater for these storms.

The importance of downdrafts in initiating and focusing deep convection is well known. For example, the essential role of the low-level "cold pool" fed by downdrafts in constraining intense convective cells to be focused along squall lines was recognized by Fujita (1959); the dynamics of the cold pool's interaction with its mesoscale environment have recently been elucidated by RWK. Our results suggest that a relationship exists between environments exhibiting relatively stable (i.e. cool and moist) low-level conditions and Weakly Classifiable or Unclassifiable MPS structure, in which convective activity might aptly be de-

[4] The mean line orientation shown (220°–40°) was determined for those periods during which line speeds (cf. Table A1) were computed. The resulting mean orientations of Symmetric and Asymmetric systems were virtually identical.

[5] We follow Bluestein and Jain (1985), who defined the convective inhibition (CIN) as the net work per unit mass required to lift a negatively buoyant air parcel from the surface to the level of free convection, i.e. the negative area between the curve defined by the parcel's temperature as a function of height and its (warmer) environment.

scribed as "unfocused." Moist, stable low-level conditions (such as those frequently observed on the cool side of a stationary- or warm-frontal boundary) would act to impede the establishment of penetrative downdrafts driven by evaporation and negative buoyancy. In their absence, development of a mesoscale cold pool (and the accompanying arclike mesoscale band of convergence along its expanding boundary) might be retarded or prevented altogether. Thus, an important ramification of more stable boundary-layer conditions might be the formation of less focused, more chaotic patterns of low-level convergence and associated convective activity. While other mechanisms undoubtedly influence observed mesoscale patterns of deep convection, our results indicate that the stratification of the lower troposphere and its interaction with downdrafts generated within mesoscale convective systems is deserving of further attention.

4) BULK RICHARDSON NUMBER

To the degree that the mesoscale organization of MPSs depends upon the nature of their constituent deep convection, we might expect this to be reflected in a parameter that combines essential characteristics of both the surrounding shear and thermodynamic stratification. Such a parameter is the bulk Richardson number, which is defined as

$$\mathrm{Ri} = \frac{\mathrm{CAPE}}{\frac{1}{2}\bar{U}^2},$$

where $\bar{U}$ is the mean density-weighted vertical wind shear in the layer between 0.5 and 6 km AGL. This parameter has been demonstrated to have profound implications relating to the structure and evolution of convective cells (Weisman and Klemp 1982). A tendency was found for the low-level inflow regions of Strongly Classifiable systems to exhibit larger values of Ri than their Weakly Classifiable counterparts, with mean Ri values of about 90 and 11, respectively (cf. Row 21 of Table 9). This considerable difference was due both to the greater shear and lesser instability associated with less classifiable systems. The value of Ri for storms exhibiting Strongly Classifiable leading-line/trailing-stratiform structure falls decidedly within the range ($\mathrm{Ri} > 40$) that Weisman and Klemp found to favor multicellular convective structure, while that for Weakly Classifiable systems lies just below the range ($15 < \mathrm{Ri} < 35$) favoring unicellular or supercell-type storms. This difference is consistent with the data in Table 6a, which show tornado frequency increasing from 1.0 to 2.6 per MPS for Strongly versus Weakly Classifiable mesoscale organization.

Perhaps because of the relatively small sample size considered, the cited difference in Ri was found to be significant at only the 75% level. While this level of confidence is too low to support any definitive statements regarding the relationship between bulk Richardson number and mesoscale storm organization, it certainly merits consideration in future studies involving larger datasets or numerical simulations of mesoscale convective systems. It is further noteworthy that the association of multicell structure with the Strongly Classifiable type of mesoscale structure is physically consistent with the results of case studies of Strongly Classifiable, leading-line/trailing-stratiform squall lines (e.g., Houze 1977; Smull and Houze 1985, 1987b; Chong et al. 1987; Rutledge et al. 1988). The formation of new cells at the front of the convective zone and continual dissipation of convective cells to the rear indeed represents an important source of water substance promoting trailing-stratiform precipitation in these storms (Gamache and Houze 1983). In environments characterized by lower Ri values, organized-multicell behavior would likely be inhibited (i.e., individual cells would be longer-lasting), thus eliminating a major impetus for the initiation and maintenance of trailing-stratiform structure.

e. Comparison of environments supporting Classifiable and Unclassifiable radar-echo structure

In section 8d, we compared classifiable cases with one another. More specifically, Strongly, Moderately, and Weakly Classifiable systems were compared in an attempt to relate features of the environments of storms to degree of organization. We now seek to distinguish environments of storms with Classifiable structure from those of storms that bore no resemblance whatsoever to the leading-line/trailing-stratiform archetype. To obtain the sharpest comparison, we consider differences between Strongly Classifiable cases (Categories 1+4), i.e. the cases with the most clearly defined leading-line/trailing-stratiform structure, and the Unclassifiable cases (Categories 7+8). Little new information is gained by including the Moderately and Weakly Classifiable cases in these comparisons.

In columns E and H of Table 9 it can be seen that in comparison to Strongly Classifiable systems, Unclassifiable ones tend to occur in the presence of stronger, more westerly mean 3–10 km winds (at the 90% significance level), lower equilibrium levels (80% significance), cooler boundary-layer conditions (although this aspect was more variable and related to severe weather production, as will be discussed in section 8h), and larger convective inhibition (80% level). The mean bulk Richardson number for Unclassifiable storms (22) lies well within the range ($15 < \mathrm{Ri} < 35$) associated with supercell convective storms, and is less than the mean Ri for Strongly Classifiable storms (90) at the 80% level of significance.

The mean hodograph for Unclassifiable systems (Fig. 19) displays strong, nearly unidirectional vertical shear with little if any evidence of a low-level jet. The unmistakable presence of the low-level jet in the case of Strongly Classifiable structure (noted in section 8d2), compared with the weakness or absence of such a fea-

ture in the environments of Unclassifiable storms, suggests that the low-level jet may be important in establishing the leading-line/trailing-stratiform structure. Its role could be dynamical, thermodynamic, or both.

This empirical relationship bears an intriguing similarity to the results of Balaji and Clark (1988) and Hauf and Clark (1989), who have simulated the initiation and growth of deep convection in the context of a surrounding field of thermally-forced shallow convection (i.e., a disturbed boundary layer) using differing shear profiles. For a curved hodograph veering 90° through the low-level mixed layer and exhibiting speed shear alone above the inversion (similar to that for our Strongly Classifiable systems), the resulting deep convective modes were organized into a series of bands. These features were approximately parallel to the mid-tropospheric shear vector. By contrast, simulations based upon a straight-line hodograph (i.e., an environment with appreciable speed shear through a deep layer but no low-level jet) produced an interference pattern in which the deep convective modes took on a chaotic, scattered, horizontal distribution. Although many complex interactions are known to occur between the initiation of deep convection and appearance of a fully developed convective system, Clark and collaborators maintain that the mode of initiation may influence the pattern of convection even into its mature stage.

To ensure that the absence of a low-level jet in the mean environment of the Unclassifiable systems seen in Fig. 19 was not a result of averaging, each of the 15 soundings in this group (Categories 7+8) was examined individually. It was found that all but one of the hodographs lacked a low-level jet, exhibiting virtually unidirectional shear. The exception was a case in which two MPSs occurred in close succession. The first was Unclassifiable, however the second was the Strongly Classifiable/Symmetric system shown in Fig. 9a.

A graphical representation of the shear for Unclassifiable systems is shown in Fig. 24c. In comparison to Strongly Classifiable (Fig. 24a) and Weakly Classifiable (Fig. 24b) cases, the Unclassifiable systems exhibit an intermediate amount of shear, with the shear at lower

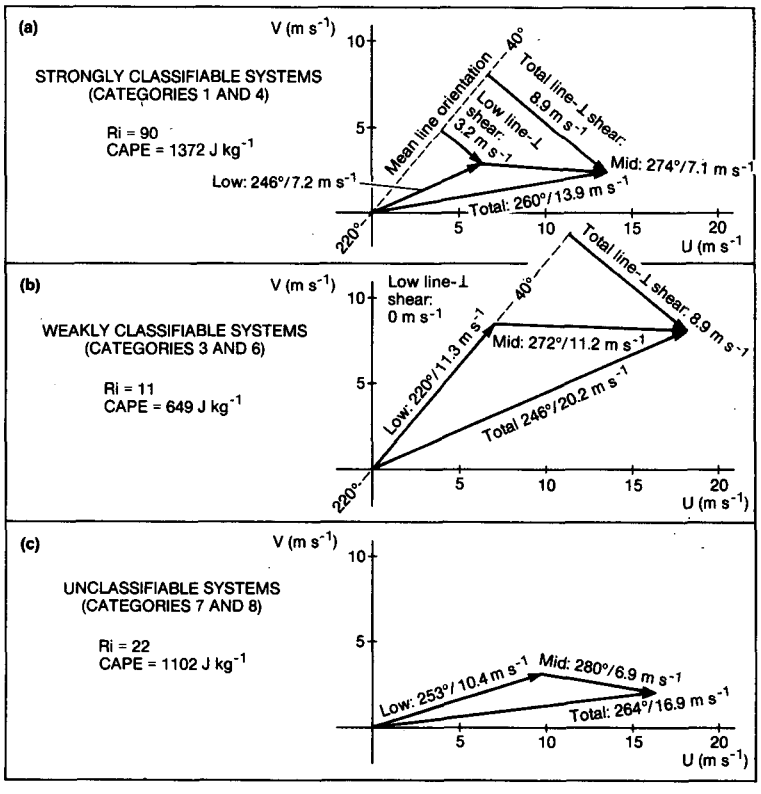

FIG. 24. Vertical wind shear associated with various types of organization of mesoscale precipitation systems (see text). U and V represent the east–west and north-south wind components, respectively. Shear vectors are shown for three layers: "Low" (Surface-2.5 km AGL), "Mid" (2.5–6.0 km AGL), and "Total" (Surface-6.0 km AGL). Where applicable, the mean squall-line orientation (220°–40°) and line-perpendicular shear are indicated. Mean values of bulk Richardson number (Ri) and convective available potential energy (CAPE) for each type of organization are also given. (a) Strongly Classifiable systems (Categories 1 and 4); (b) Weakly Classifiable systems (Categories 3 and 6); Unclassifiable systems (Categories 7 and 8).

levels being somewhat stronger than that at midlevels (Figs. 19 and 24c).

f. Comparison of environments supporting Symmetric and Asymmetric radar-echo structure

In section 8d, we examined the environments of Classifiable mesoscale systems with respect to the degree to which they exhibited leading-line/trailing-stratiform structure, regardless of whether that structure was of the Symmetric or Asymmetric type. We now seek to identify environmental differences between cases which displayed Symmetric and Asymmetric structure, regardless of the degree to which they were Classifiable. Thus, we compare the mean sounding for all Classifiable/Symmetric cases (Categories 1+2+3, Fig. 22, column I of Table 9) with that for all Classifiable/Asymmetric cases (Categories 4+5+6, Fig. 23, column J of Table 9). The wind shear for these two groups is graphically summarized in Fig. 25.

Few statistically significant differences are found between environments of MPSs exhibiting Symmetric versus Asymmetric structure. The 3–10 km mean wind speed and 0–6 km vertical shear are somewhat stronger for environments of Asymmetric systems, at the 75% and 90% significance levels, respectively. No significant differences in thermodynamic attributes or bulk Richardson number are indicated.

The hodographs in Figs. 22 and 23 show that the low-level jet is sometimes present in both Symmetric and Asymmetric cases. Figure 25 illustrates that the greater shear accompanying the Asymmetric cases is principally in the along-line direction. In section 8d(2), we noted a similar result in the comparison of Strongly and Weakly Classifiable cases (cf. Figs. 24a,b and 25a,b). We suggested that in the Weakly Classifiable cases, the stronger along-line component of shear favors development of supercells along the line, thus giving it an irregular, less classifiable character. We now further suggest that, when the along-line shear is strong, the supercellular formation may be especially favored on the southwestern end of the line, giving the line an asymmetric aspect (as indicated in Fig. 8).

As noted by RWK, the effectively infinite length of simulated squall lines (resulting from the use of periodic boundary conditions in the along-line direction, a choice mandated by computational constraints) precludes representation of some physical processes peculiar to lines of finite length. For example, depending upon their distance from the end of the line, convective cells may respond differently to the ambient shear profile. Cells at or near to the south or southwest end of a line may experience the ambient shear in a manner similar to that of an isolated convective cell. They are exposed to the full effect of the shear—not just the line-normal component. The strong shear near the end of the line would favor development of supercell convective structure. However, owing to interactions with adjacent cells and the system-scale circulation, cells farther up the line would be affected principally by the line-normal shear component (M. Weisman, personal communication). Since this shear component is relatively weak ("suboptimal" in the terminology of RWK), the downwind (northeastern) portion of the line takes on a multicellular structure and develops a rearward tilt and trailing-stratiform region. This effect, together with the fact that the downwind end of the line is simply older, implies that the centroid of the stratiform region should be located behind the down-

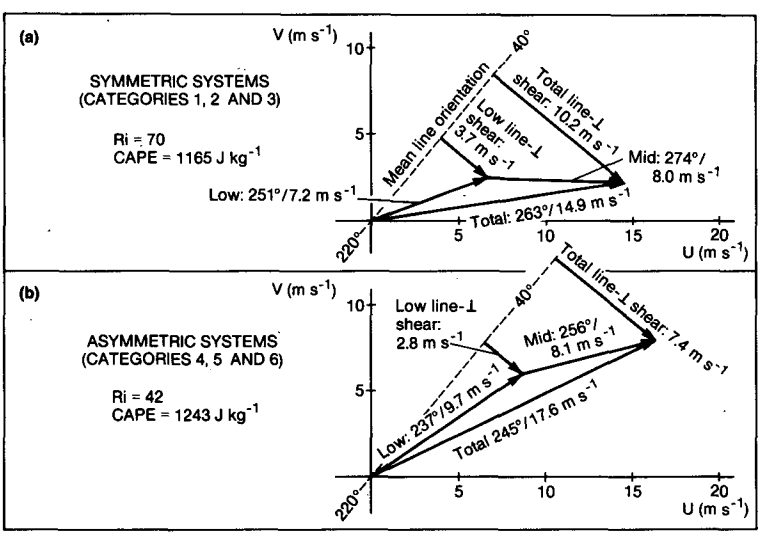

FIG. 25. As in Fig. 24, except for (a) Symmetric systems (Categories 1, 2 and 3), and (b) Asymmetric systems (Categories 4, 5 and 6).

wind portion of the line—well removed from the most intense convection. In this manner, asymmetric structure is introduced, both with respect to the convective structure of the line and to the placement of the stratiform area relative to the line (both of which enter into the symmetry parameter "S").

Finally, we note that the supercellular structure at the southwestern extremity of the line is not the only possible explanation for Asymmetric radar-echo structure. As discussed by Houze et al. (1989), it is not uncommon for a mesoscale vortex to form at midtropospheric levels in the stratiform regions of mesoscale convective systems. This vortex promotes asymmetric precipitation structure of the type depicted in Fig. 8 by importing dry midlevel air into the southern half of the system from the rear and advecting cloud and precipitation from the convective line rearward into the northern half of the system.

g. Comparison of environments supporting Unclassifiable radar-echo structure with and without high numbers of severe weather reports

According to Table 3, one-third of the mesoscale precipitation features in the major rain events (21 of 63) were found to have Unclassifiable radar-echo structure, i.e. no resemblance to the leading-line/trailing-stratiform type of organization. Because of their complex character, no attempt was made to subdivide the Unclassifiable cases according to echo structure. However, one natural subdivision that suggests itself is according to severe weather occurrence. According to Table 5c, eight of the Unclassifiable cases produced ten or more reports of severe weather. These are grouped together here in Category 7 and referred to as Unclassifiable/Severe. The remainder of the cases are combined in Category 8, referred to as Unclassifiable/Nonsevere. The soundings for Categories 7 and 8 are in Figs. 20 and 21. Parameters derived from the soundings are in columns J and K of Table 8.

Environments of the Unclassifiable/Severe cases on average possessed stronger and deeper vertical wind shear. For the 2.5–6 km layer, this difference was significant at the 90% level. Their mean winds were also stronger and more westerly, also at the 90% level. Surprisingly, values of CAPE for these two groups were quite similar. However, the contrast of certain other thermodynamic measures was more remarkable. Relatively warm and less humid low-level conditions accompanying the more severe MPSs led to a significantly higher mean lifting condensation level (LCL); this finding was significant at the 99% level. That is to say, higher cloudbases and greater potential for subcloud evaporation accompanied the more severe systems (both in terms of depth of the unsaturated layer and degree of subsaturation). Insofar as the potential for subcloud evaporation is a valid predictor of convective downdraft strength (e.g., Foster 1958), this relationship is reasonable.

Another intriguing result is that the convective inhibition (CIN) for the more severe systems in Category 7 was on average less than that for those Unclassifiable/Nonsevere systems. While the confidence level for this difference is quite low (50%), it mirrors the statistically significant results of Bluestein et al. (1987), who compared the environments of severe versus nonsevere squall lines and found appreciably lower values of CIN for severe cases. The mean temperature in the lowest 500 m was higher by 4°C (at the 95% confidence level) for the environments of Unclassifiable/Severe cases. Examination of data for all eight basic groups (columns D–K of Table 8) reveals that Unclassifiable/Nonsevere storms were associated with some of the coldest boundary-layer temperatures observed during major rain events, being 3.5°C cooler on average than those in Category 1 (at the 98% confidence level).

h. Characteristics of environments supporting types of radar-echo structure associated with high numbers of severe weather reports

From the data presented in Tables 5a–c (section 6) and the discussion in section 8g, three particular types of radar-echo organization stand out as being especially prolific producers of severe weather. These types (along with their corresponding sounding analysis category and dominant type of severe weather) can be denoted as follows:

Type I	Strongly Classifiable/Symmetric [esp., flooding (Table 6f)]
Type II	Moderately and Weakly Classifiable/Asymmetric [esp., tornadoes and hail (Table 6a and c, respectively)]
Type III	Unclassifiable/Severe [esp., much hail (Table 6c)]

Examination of the soundings for these three groupings indicates the environmental characteristics of mesoscale precipitation systems that produced the most severe weather. We represent Type I by combining sounding Categories 1 and 2, Type II by Categories 5 and 6, and Type III by Category 7. Differences in the wind shear and Bulk Richardson number for these groupings can be derived from Table 8 and are illustrated graphically in Fig. 26.

The mean Ri is 79 and thus is in the multicell range for the Type I cases. The values for Type II and III are 45 and 25, respectively, and thus either border or lie within the supercell range. These values might be expected since the severe weather in Type I cases tends to be associated more strongly with flooding than storms with probable rotational characteristics. We have already noted (section 8d) the consistency of multicellular convection with the leading-line/trailing-stratiform structure. The Type II and III mesoscale systems are, on the other hand, more prolific producers

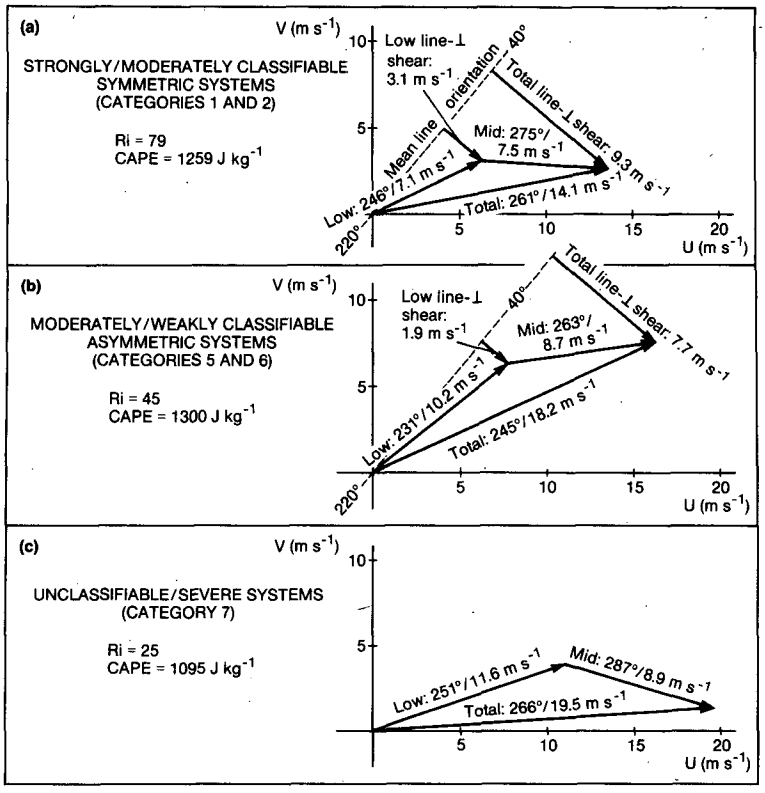

FIG. 26. As in Fig. 24, except for (a) Strongly and Moderately Classifiable/Symmetric systems (Categories 1 and 2), (b) Moderately and Weakly Classifiable/Asymmetric systems (Categories 5 and 6), and (c) Unclassifiable/Severe systems (Category 7).

of tornadoes and hail, which are typically associated with rotating supercell thunderstorms.

Figure 26 indicates that the shear tended to be of a different character in each of the three types of mesoscale organization associated with severe weather. The Type I cases were characterized by weaker shear at a relatively large angle to the mean line orientation. The Type II cases were characterized by stronger shear in the along-line direction. The Type III cases, which being Unclassifiable exhibit no line structure, also have a strong shear, but from a westerly direction compared to the southwesterly direction characterizing the Type I and II cases.

In summary, the cases of frequent flooding tend to be associated with Strongly Classifiable Symmetric mesoscale radar-echo organization in environments with weak low-to-mid tropospheric southwesterly shear oriented at a relatively large angle to the line, with a low-level jet, and characterized by a Ri in the multicellular storm range. The highest frequency of tornadic storms tended, in contrast, to occur in association with Moderately to Weakly Classifiable/Asymmetric mesoscale organization in the presence of stronger, southwesterly, but more along-line shear, with a strong low-level jet and with Ri near the supercell range. The severe weather (mostly hail) in the Unclassifiable/Severe category of mesoscale organization tended to occur in strong, unidirectional, westerly shear absent from any sign of a low-level jet, with Ri well within the supercellular range.

9. Conclusions

Examination of six years of radar data collected during springtime in central Oklahoma has allowed us to develop a climatology of the types of mesoscale organization exhibited by rainstorms that occur in this important setting. These findings are significant not only as they relate to precipitation and severe weather over the Plains States, but because they are likely representative of midlatitude mesoscale convective systems in a broader context. As noted in the Introduction, selected case studies have emphasized two types of squall line organization that occur in midlatitude mesoscale convective storms: 1) the symmetric leading-line/trailing-stratiform (ll/ts) structure noted by Newton (1950), Fujita (1955), Pedgley (1962), and others; and 2) the asymmetric ll/ts structure described by Newton and Fankhauser (1964). More recently, Bluestein and Jain (1985) and Bluestein et al. (1987) have examined modes of squall line formation. They did not, however, consider the whole range of precipitating mesoscale

systems, and their statistics included lines that were not necessarily associated with significant widespread rainfall.

We have focused not on the question of line formation but rather on the nature of mesoscale organization evident in the precipitation structure of these storms. More specifically, to bring this question into sharper focus, we considered only storms associated with major precipitation events—defined as occurrences of $\geq$25 mm of rain over an area of $\geq$12 500 km^2 during a 24-h period. Operational meteorologists have long recognized that convective systems exhibit a wide variety of structures, and that the radar-echo patterns during heavy rain episodes sometimes do not show any tendency toward line formation, or perhaps only show a rather temporary linear organization that devolves to a more chaotic appearance. However, these general impressions have remained largely undocumented. The approach described in this paper has yielded a more orderly, measured, and comprehensive description of the types of mesoscale organization that occur in midlatitude rainstorms than has previously been available.

The first important result that emerges from careful examination of radar data for a six-year period is that large areas of stratiform precipitation consistently occur in connection with areas and lines of deep convective cells during major rain events. The primary rain area of a typical storm is a contiguous region of precipitation tens to hundreds of kilometers in scale that consists partly of deep convective cells and partly of stratiform rain. On average the stratiform portion alone reached $\approx$30 000 km^2 in area.

Since large convective and stratiform components made up each mesoscale rain area, it was convenient to classify the mesoscale organization of each storm in terms of the horizontal juxtaposition of these components. The highest degree of organization was considered to be the ll/ts structure described in several previous case studies. Characteristics of this type of organization have been identified and incorporated into schematic models (Figs. 7 and 8). These models indicate two subforms of ll/ts structure, "Symmetric" and "Asymmetric."

The mesoscale precipitation systems (MPSs) contributing to major rain events were examined individually. An MPS was deemed "Classifiable" if it exhibited any perceptible similarity to either of the forms of ll/ts radar-echo structure indicated in the schematic models. MPSs that bore no resemblance whatsoever to the models in Figs. 7 and 8 were termed "Unclassifiable." We found 42 of the MPSs were Classifiable, while 21 were Unclassifiable. This result indicates that in two-thirds of the MPSs there was some tendency toward ll/ts structure. However, of the 42 Classifiable cases, only 14 were deemed to bear a strong similarity to the idealized models. Moreover, these 14 cases exhibited a continuum of organizations distributed fairly evenly between the Symmetric and Asymmetric alternatives of ll/ts structure. The MPSs that were only moderately or weakly similar to the idealized ll/ts models were also distributed fairly evenly between the Symmetric and Asymmetric forms. Thus, a comprehensive examination of radar-echo patterns leads to the conclusion that while a majority of MPSs comprising the major rain events exhibit at least some tendency toward ll/ts structure, they occur in a continuous spectrum of degree of mesoscale organization, ranging from Strongly Classifiable (i.e., unmistakable ll/ts structure) through Weakly Classifiable to completely Unclassifiable, with a superposed variation from the Symmetric to Asymmetric type evident in the Classifiable cases.

Although the MPSs evince a continuous spectrum of mesoscale organization, certain radar-echo patterns stand out as being particularly important in terms of severe weather. About half of Oklahoma's springtime severe weather during the six-year study period occurred in association with major rain events, with most (89%) of that occurring during major rain events being located within the confines of radar echoes constituting MPSs. The bulk of severe weather reported in the MPSs was, in turn, found within their convective portions (the exception being floods, which were sometimes associated with stratiform regions). In agreement with previous studies (e.g., Maddox 1980), we found that severe weather reports—especially hail and tornadoes—were most numerous during the early stages of these systems. However, other types of severe weather such as high winds and flooding, which are associated not only with severe convective cells but also occur in concert with mature-stage MPS features (e.g., extensive gust fronts accompanying bow-echo patterns, protracted and widespread rainfall, etc.), were distributed more evenly throughout their life cycles.

Classifiable and Unclassifiable MPSs were equally likely to have attendant severe weather. They each averaged between 7 and 8 severe weather reports per system. However, the number of reports in individual MPSs varied widely, with a tendency for severe weather to be concentrated in "outbreaks" in which a large number of reports (10–40) were produced by a single system. Tornadoes were slightly more frequent in MPSs with Classifiable echo structure, while damaging hail was much more frequent in the Unclassifiable MPSs.

Among the Classifiable MPSs, the systems that produced the greatest number of severe weather reports were those exhibiting Moderately to Weakly Classifiable/Asymmetric (moderate-C, low-S) organization. These storms resemble the type of squall line described by Newton and Fankhauser (1964). This type of MPS typically takes the form of a southwest–northeast oriented echo region that is narrow and intensely convective (with large, irregularly shaped cells) at its southwest end, while its northeastern extremities are broader and more stratiform. The second-ranking cat-

egory of mesoscale organization in terms of severe weather production among the Classifiable cases was the Strongly Classifiable/Symmetric (high-C, high-S) type. Thus, when the complete spectrum of mesoscale organizations is examined, the result is obtained that the types of squall lines focused on in early studies emerge as two of the categories of mesoscale structure characterized by the greatest frequency of severe weather.

The third category of mesoscale organization that produced large amounts of severe weather was the Unclassifiable/Severe category. However, by definition, these systems do not exhibit line structure and hence do not relate to any previous case studies of squall lines.

There were important differences in the nature of severe weather among the three categories of storm organization characterized by numerous severe weather reports. Strongly Classifiable/Symmetric storms were characterized by the highest frequency of flood reports, while those in the Moderately to Weakly Classifiable/Asymmetric categories had the highest frequency of tornado and hail reports. The Unclassifiable/Severe cases were just as active in producing severe hail as the "Newton-Fankhauser type" asymmetric lines, but were not as prolific in terms of tornadoes.

The importance of mesoscale convective complexes (Maddox 1980) in producing precipitation has been quantified by Fritsch et al. (1986), who showed that over half of the warm season rain in the central United States comes from these systems. Major rain events, as defined here, were virtually always recorded when an MCC passed over the study area (the only exceptions being when the MCC was in its dissipating stage or merely skirting the area). On the other hand, most ($\approx$75%) of the major rain events stemmed from cloud shields that failed to meet the MCC criteria, although in many cases they took on an qualitatively similar appearance. Since MCCs are defined in terms of the character of upper-level cloud shields depicted in satellite imagery, the mesoscale organization of the underlying precipitation has not previously been established (other than in a few case studies). Our examination of the radar echoes during major rain events indicates no strong tendency for any particular structure to be preferred in MCCs; a broad spectrum of structures, including squall-line systems of the ll/ts type, was observed beneath MCC cirrus canopies. The tabulations revealed a slight tendency (but one of questionable statistical significance) for Unclassifiable (chaotic) precipitation patterns to be favored over more organized linear structures in MCCs.

Routine synoptic soundings taken in advance of MPSs responsible for major rain events were often located far from the mesoscale systems in space and time. Nonetheless, they provided a limited description of the mean large-scale conditions associated with the occurrence of the various forms of mesoscale organization. The main results gained from the examination of these soundings can be briefly summarized as follows.

The environments of Strongly Classifiable mesoscale rain areas, i.e. those with sharply defined ll/ts structure, are characterized by bulk Richardson numbers (Ri) typical of multicell development. The environments of Weakly Classifiable mesoscale systems exhibited stronger shear and Ri values characteristic of supercell storm organization. These differences between the environments of Strongly and Weakly Classifiable mesoscale systems are consistent with the higher frequency of tornado occurrence in the Weakly Classifiable structures and with observations from case studies, which indicate that the convection in the lines of Strongly Classifiable systems behaves in an organized-multicellular manner (e.g., Smull and Houze 1985; 1987a,b).

The sounding data are also consistent with the model results of RWK and Fovell and Ogura (1988, 1989), who find that lower tropospheric shear normal to the line, of the magnitude observed in our cases, favors the type of squall line that evolves quickly toward ll/ts structure. The environments of both the Strongly and Weakly Classifiable systems (Symmetric and Asymmetric) were characterized by line-normal shear of about 10 m s^{-1} through the lowest 6 km of the troposphere.

The Weakly Classifiable/Asymmetric mesoscale systems were characterized by greater along-line shear, which apparently favored discrete, supercell-type convection, especially on the upwind end of these "Newton-Fankhauser" type lines. The preferential development of intense convective features on the upwind end apparently tended to give the lines an asymmetric appearance. Moreover, the presence of supercells would account for the relatively high frequency of tornadic activity identified with this type of Classifiable mesoscale structure (Table 6a). The confinement of stratiform precipitation to only that region behind the downwind section of the line evidently reflects the greater age of this part of the storm and that this part of the line is responding primarily to the cross-line component of shear, which favors the trailing-stratiform type of structure.

The appearance of Unclassifiable radar-echo structure was typically accompanied by Ri values in the supercell range. The environments of these storms differed most notably from the Classifiable cases in that there was no evidence of a low-level jet. Since the key factor differentiating Unclassifiable from Classifiable structure is the absence of any sort of convective line to which other features can be related, it is suggested that the low-level jet in some way encourages line organization. The absence of a low-level jet also may relate to the severe weather observations. Although much hail was observed in association with Unclassifiable systems (Table 6c) and the responsible convective cells often "looked" to us as though they were

supercells, tornado frequency was not as common as in Classifiable storms—especially the Moderately to Weakly Classifiable/Asymmetric cases (Table 6a). The absence of a low-level jet in conjunction with Unclassifiable cases may be responsible not only for the lack of line organization in the MPSs, but also for the lower frequency of tornado reports in this category. The role of increased hodograph curvature (such as that produced by a low-level jet) in contributing to the large helicity (Lilly 1983) associated with *tornadic* supercell storms has been discussed by Davies-Jones (1984).

When the forms of mesoscale organization characterized by severe weather were examined, it was found that the Classifiable/Symmetric mesoscale organization, which favors flooding, was characterized by low-to-middle tropospheric southwesterly shear oriented at a sharp angle to the line, a low-level jet, and Ri in the multicellular storm range. The Moderately to Weakly Classifiable mesoscale organization, which favored both tornadoes and hail, occurred in the presence of stronger, southwesterly, but more along-line shear, with a strong low-level jet and with Ri in or just below the supercell range. The Unclassifiable/Severe category of mesoscale organization, which favored reports of hail but not particularly tornadoes, tended to occur in strong, unidirectional, westerly shear, with no low-level jet and Ri values well within the supercellular range. At present, no clear analog to the Unclassifiable type of organization in numerical simulations has been reported.

We hope that the radar-echo classification scheme and documented characteristics of convective systems responsible for major springtime rain events over Oklahoma during a six-year period will provide a useful framework within which future case studies may be evaluated and against which expanded climatological studies may be compared. We also hope that these results are of some use in guiding the application of diagnostic and prognostic numerical models in illuminating the dynamics and effects of mesoscale convective systems.

APPENDIX

Tabulation of Characteristics of Mesoscale Precipitation Systems

In order to classify each Mesoscale Precipitation System (MPS) according to the scheme outlined in section 5, a matrix was constructed as shown in Table A1. Each row corresponds to one of the 69 MPSs, while columns B–K and M–N correspond to one of the characteristics of leading-line/trailing-stratiform (ll/ts) precipitation structure enumerated in section 4. In other columns of the table, ancillary data regarding severe weather reports, MCC characteristics, etc., have been entered. The date in column A corresponds to the particular major rain event (as listed in Table 2). In those major rain events where multiple MPSs passed over the study area during the 24-h period, systems are denoted by (1), (2), . . . , following the date in the order of their appearance. Columns B–K contain the ten basic characteristics of ll/ts structure, as listed in section 4, while columns M and N contain the characteristics that determine whether the MPS more closely resembles the Symmetric Case or the Asymmetric Case type of ll/ts structure (also described in section 4). Elements in these columns of the matrix were assigned the following designations, based on our evaluation of the echo structure:

1	Indicates the *characteristic* (defining a *column* of the matrix) was observed unambiguously in a particular *MPS* (defining the *row* of the matrix)
0.5	Characteristic seemed to be present in the MPS but the analyst had some doubt
−1	Characteristic definitely not observed in the MPS
−0.5	Characteristic seemed not to be present in the MPS but the analyst had some doubt
0	Particular characteristic was indeterminable from the available data
U	The radar-echo pattern of the MPS being evaluated bore so little resemblance to either type of ll/ts organization that no attempt was made to apply any of the above designations. Instead, all columns pertaining to system structure in the row of the matrix corresponding to that MPS were designated as "U," signifying that the system was "Unclassifiable" in relation to the Symmetric or Asymmetric Case
B	The radar data for the MPS being evaluated were incomplete or otherwise inadequate to determine whether or not the system resembled the Symmetric or Asymmetric Case. An entry of "B," signifying "bad data," was thus made in all columns pertaining to storm structure in that row.

Several factors could lead to the "bad data" designation. The most common was that the radar film was of such low quality as to render detailed examination and tabulation of structural characteristics impossible, although the presence (or absence) of radar echo could generally be determined. If a MPS merely skirted the study area (e.g., as revealed by satellite imagery), the radar data were considered inadequate to attempt classification.

After all of the elements in columns B–K and M–N of Table A1 were filled in, a score C was calculated for each classifiable MPS (i.e., for each row of the matrix other than those rows containing U or B designations). This quantity is given by

C = Sum of the positive and negative numbers recorded

TABLE A1. Mesoscale Precipitation Systems (MPSs, one per row) observed during major rain events (MREs). Column A designates MRE date on which the MPS occurred; if more than one MPS passed over study area during the 24-h period corresponding to the MRE, individual MPSs are denoted (1), (2), ... Columns B–O list attributes of mesoscale precipitation structure (described in text). Entries "U" and "B" designate to "Unclassifiable" structure and "Bad Data," respectively. Column P lists total number of severe weather events reported in study area (defined in text) during the passage of each MPS; these are subdivided by type in Columns Q–W. In Column X, a "Yes" entry indicates that the MPS occurred beneath a cloud shield that qualified as a mesoscale convective complex (MCC). Column Y gives the date and time of the representative environmental sounding at Oklahoma City; "N/A" indicates that no appropriate sounding was available (see text).

TABLE A1—PART I

	A	B	C	D	E	F	G	H	I
1	MPS	Leading Line	Leading Line	Leading Line	Leading Line	Leading Line	Leading Line	Leading Line	Strat. Region
2	Designator	Shape	Solid	Orientation	Speed	Strong Refl.	Edge Serrated	Cells Elongated	Size >
3		Arc-like				Gradient		45-90°to line	10**4km**2
4	77/4/21	-1	1	1	-0.5	1	0.5	0.5	1
5	77/5/02	U	U	U	U	U	U	U	U
6	77/5/17	1	1	1	0.5	1	1	1	1
7	77/5/20	-1	1	1	0.5	1	-1	-1	1
8	77/5/21(1)	0.5	-1	1	-1	-1	-1	-1	0.5
9	77/5/21(2)	1	1	1	0.5	0.5	-0.5	-0.5	0
10	77/5/21(3)	1	1	1	1	1	-0.5	1	1
11	77/5/27	-1	1	1	1	1	1	0.5	1
12	78/4/10(1)	1	-1	1	-0.5	1	0.5	0.5	-1
13	78/4/10(2)	U	U	U	U	U	U	U	U
14	78/5/03	-1	-1	-1	0	0	-1	-1	1
15	78/5/20	-1	-1	1	1	1	0.5	0.5	1
16	78/5/21	U	U	U	U	U	U	U	U
17	78/5/27	1	1	1	0.5	1	1	1	1
18	78/5/28	-1	1	1	0.5	1	0	-1	1
19	78/6/05	1	1	1	1	1	1	0.5	1
20	78/6/06(1)	B	B	B	B	B	B	B	B
21	78/6/06(2)	-0.5	1	1	1	1	0.5	-1	1
22	78/6/22(1)	-1	1	1	1	-1	-1	-1	-1
23	78/6/22(2)	B	B	B	B	B	B	B	B
24	79/4/11	-1	-1	1	0.5	-1	-1	1	1
25	79/5/03(1)	-1	1	0.5	0.5	1	-1	0.5	1
26	79/5/03(2)	-1	-1	0	0	-1	-1	-1	0
27	79/5/03(3)	-1	-1	1	1	-1	-0.5	-0.5	1
28	79/5/21(1)	U	U	U	U	U	U	U	U
29	79/5/21(2)	1	1	1	0	1	0.5	0.5	1
30	79/5/22	U	U	U	U	U	U	U	U
31	79/6/09(1)	-1	1	1	-0.5	1	0.5	-1	1
32	79/6/09(2)	1	1	1	1	1	1	0.5	1
33	80/4/24(1)	1	1	1	-0.5	1	0.5	0	1
34	80/4/24(2)	1	-1	-1	1	1	0.5	0.5	-1
35	80/4/25(1)	U	U	U	U	U	U	U	U
36	80/4/25(2)	U	U	U	U	U	U	U	U
37	80/4/26	U	U	U	U	U	U	U	U
38	80/5/02(1)	U	U	U	U	U	U	U	U
39	80/5/02(2)	0	-1	0.5	-0.5	0.5	0	0.5	1
40	80/5/15	B	B	B	B	B	B	B	B
41	80/5/16	B	B	B	B	B	B	B	B
42	80/5/18	U	U	U	U	U	U	U	U
43	80/5/27	B	B	B	B	B	B	B	B
44	80/5/29(1)	1	1	1	1	1	-1	-1	-1
45	80/5/29(2)	-1	1	1	1	1	-1	-1	-1
46	80/5/30	U	U	U	U	U	U	U	U
47	80/6/17	U	U	U	U	U	U	U	U
48	80/6/19	U	U	U	U	U	U	U	U
49	80/6/20(1)	U	U	U	U	U	U	U	U
50	80/6/20(2)	-1	-1	1	1	0.5	-1		-1
51	80/6/20(3)	0.5	0.5	1	1	1	-1	-1	1
52	80/6/20(4)	1	1	1	1	1	-1	-1	-1
53	81/5/09(1)	U	U	U	U	U	U	U	U
54	81/5/09(2)	0.5	0.5	1	1	-1	-1	-1	1
55	81/5/24	U	U	U	U	U	U	U	U
56	81/5/29(1)	U	U	U	U	U	U	U	U
57	81/5/29(2)	U	U	U	U	U	U	U	U
58	81/5/30	0.5	-1	1	-0.5	1	-1	-1	-1
59	81/6/02	1	1	1	1	1	1	1	1
60	81/6/03	1	-1	1	0.5	1	-1	-1	1
61	81/6/15	1	1	1	1	0	1	1	0
62	81/6/16	B	B	B	B	B	B	B	B
63	82/5/06	0.5	1	1	-0.5	1	1	0	1
64	82/5/12	1	1	1	-0.5	-1	0	0	1
65	82/5/16	U	U	U	U	U	U	U	U
66	82/5/17	0.5	1	1	1	1	1	1	1
67	82/5/24(1)	-1	-1	1	0.5	0	0	0	-1
68	82/5/24(2)	-1	1	1	-0.5	0	0	0	1
69	82/5/28	1	1	1	1	1	-1	0.5	1
70	82/6/16	U	U	U	U	U	U	U	U
71	82/6/24(1)	U	U	U	U	U	U	U	U
72	82/6/24(2)	1	1	1	1	0	0	0	1

TABLE A1—PART II

	A	J	K	L	M	N	O	P	Q
1	MPS	Strat. Region	Strat. Region	Leading-Line/	Leading Line	Strat. Region	Symmetric vs.	Total Severe	Tornadoes
2	Designator	Notch	Secondary Refl	Trailing-Strat	Convection	Location	Asymmetric	Weather	
3			Maximum	Score 'C'	Not Biased	Centered	Score 'S'	Reports	
4	77/4/21	0	1	4.5	1	1	2	8	0
5	77/5/02	U	U	U	U	U	U	9	0
6	77/5/17	0	-1	6.5	-1	1	0	2	0
7	77/5/20	-0.5	0.5	1.5	-1	-1	-2	15	3
8	77/5/21(1)	-1	-0.5	-4.5	-1	-1	-2	28	13
9	77/5/21(2)	0	-0.5	2.5	1	1	2	2	0
10	77/5/21(3)	1	1	8.5	1	-0.5	0.5	8	3
11	77/5/27	-1	1	5.5	-0.5	1	0.5	3	0
12	78/4/10(1)	0.5	1	3	-0.5	-1	-1.5	1	0
13	78/4/10(2)	U	U	U	U	U	U	0	0
14	78/5/03	-1	1	-4	0	1	1	0	0
15	78/5/20	0	1	4	0.5	-1	-0.5	1	0
16	78/5/21	U	U	U	U	U	U	0	0
17	78/5/27	-0.5	1	8	1	0.5	1.5	0	0
18	78/5/28	0.5		3	-1	-1	-2	11	1
19	78/6/05	1	1	9.5	1	-1	0	0	0
20	78/6/06(1)	B	B	B	B	B	B	3	0
21	78/6/06(2)	1	1	6	-1	-1	-2	0	0
22	78/6/22(1)	-1	-1	-4	1	-1	0	5	0
23	78/6/22(2)	B	B	B	B	B	B	0	0
24	79/4/11	-1	0.5	-1	-1	-1	-2	33	13
25	79/5/03(1)	-1	0	1.5	-1	-1	-2	39	6
26	79/5/03(2)	-1	-1	-7	-1	-1	-2	7	0
27	79/5/03(3)	-1	1	-1	-1	-1	-2	0	0
28	79/5/21(1)	U	U	U	U	U	U	3	0
29	79/5/21(2)	0.5	1	7.5	1	-1	0	1	0
30	79/5/22	U	U	U	U	U	U	0	0
31	79/6/09(1)	-1	1	2	1	1	2	4	1
32	79/6/09(2)	-1	1	7.5	1	-1	0	0	0
33	80/4/24(1)	1	-1	5	1	1	2	0	0
34	80/4/24(2)	-1	1	1	1	1	2	0	0
35	80/4/25(1)	U	U	U	U	U	U	3	1
36	80/4/25(2)	U	U	U	U	U	U	0	0
37	80/4/26	U	U	U	U	U	U	0	0
38	80/5/02(1)	U	U	U	U	U	U	13	0
39	80/5/02(2)	0.5	1	2.5	1	1	2	0	0
40	80/5/15	B	B	B	B	B	B	1	0
41	80/5/16	B	B	B	B	B	B	1	0
42	80/5/18	U	U	U	U	U	U	12	0
43	80/5/27	B	B	B	B	B	B	6	0
44	80/5/29(1)	-1	1	2	-1	-1	-2	7	0
45	80/5/29(2)	-1	1	0	1	-1	0	0	0
46	80/5/30	U	U	U	U	U	U	19	2
47	80/6/17	U	U	U	U	U	U	17	1
48	80/6/19	U	U	U	U	U	U	18	0
49	80/6/20(1)	U	U	U	U	U	U	3	0
50	80/6/20(2)	-1	1	-1.5	-1	-1	-2	4	0
51	80/6/20(3)	0	1	4	1	-1	0	5	0
52	80/6/20(4)	-1	-1	0	1	-1	0	2	0
53	81/5/09(1)	U	U	U	U	U	U	2	0
54	81/5/09(2)	-0.5	-1	-0.5	1	-1	0	0	0
55	81/5/24	U	U	U	U	U	U	15	6
56	81/5/29(1)	U	U	U	U	U	U	7	0
57	81/5/29(2)	U	U	U	U	U	U	4	1
58	81/5/30	-1	1	-2	0	-1	-1	0	0
59	81/6/02	1	1	10	-1	1	0	18	1
60	81/6/03	1	1	3.5	1	-1	0	6	0
61	81/6/15	0	0	6	1	0	1	4	2
62	81/6/16	B	B	B	B	B	B	2	0
63	82/5/06	0	1	6	-0.5	-1	-1.5	6	1
64	82/5/12	-1	1	2.5	-0.5	-1	-1.5	22	10
65	82/5/16	U	U	U	U	U	U	18	7
66	82/5/17	0	1	8.5	1	1	2	39	3
67	82/5/24(1)	0.5	-1	-2	1	-1	0	0	0
68	82/5/24(2)	0	0	1.5	1	-1	0	1	0
69	82/5/28	0	1	6.5	1	0	1	23	4
70	82/6/16	U	U	U	U	U	U	7	1
71	82/6/24(1)	U	U	U	U	U	U	11	0
72	82/6/24(2)	1	1	7	0	-1	-1	2	0

TABLE A1—PART III

	A	R	S	T	U	V	W	X	Y
1	MPS	Funnel Clouds	Hail	High Wind	Lightning	Flooding	Heavy Rain	Qualifies As	Representative
2	Designator							MCC	Sounding @ OKC
3	YY/M/DD								YY/M/DD TT(UTC)
4	77/4/21	6	0	0	1	1	0	No Data	77/4/21 00
5	77/5/02	1	6	1	0	1	0	No Data	77/5/02 00
6	77/5/17	0	0	0	0	2	0	No Data	77/5/17 00
7	77/5/20	0	2	2	2	6	0	No Data	77/5/19 12
8	77/5/21(1)	1	3	3	1	7	0	No Data	77/5/21 00
9	77/5/21(2)	0	1	0	0	1	0	No Data	N/A
10	77/5/21(3)	1	0	2	0	1	1	No Data	N/A
11	77/5/27	0	0	3	0	0	0	No Data	77/5/27 00
12	78/4/10(1)	1	0	0	0	0	0	No	78/4/10 00
13	78/4/10(2)	0	0	0	0	0	0	No	N/A
14	78/5/03	0	0	0	0	0	0	Yes	N/A
15	78/5/20	1	0	0	0	0	0	No	78/5/20 00
16	78/5/21	0	0	0	0	0	0	No	78/5/20 12
17	78/5/27	0	0	0	0	0	0	Yes	78/5/27 00
18	78/5/28	4	0	2	0	1	3	No	78/5/28 00
19	78/6/05	0	0	0	0	0	0	No	78/6/05 00
20	78/6/06(1)	1	0	0	2	0	0	No	B
21	78/6/06(2)	0	0	0	0	0	0	No	78/6/06 00
22	78/6/22(1)	0	1	4	0	0	0	Yes	78/6/21 12
23	78/6/22(2)	0	0	0	0	0	0	No	B
24	79/4/11	2	6	12	0	0	0	No	N/A
25	79/5/03(1)	6	17	10	0	0	0	No	79/5/03 00
26	79/5/03(2)	3	2	2	0	0	0	No	79/5/03 12
27	79/5/03(3)	0	0	0	0	0	0	No	N/A
28	79/5/21(1)	0	1	1	0	0	1	No	79/5/20 12
29	79/5/21(2)	0	0	0	0	0	1	No	N/A
30	79/5/22	0	0	0	0	0	0	No	N/A
31	79/6/09(1)	0	0	0	0	3	0	No	79/6/08 12
32	79/6/09(2)	0	0	0	0	0	0	No	N/A
33	80/4/24(1)	0	0	0	0	0	0	No	80/4/24 00
34	80/4/24(2)	0	0	0	0	0	0	No	80/4/24 12
35	80/4/25(1)	0	2	0	0	0	0	No	80/4/25 00
36	80/4/25(2)	0	0	0	0	0	0	No	80/4/25 12
37	80/4/26	0	0	0	0	0	0	No	N/A
38	80/5/02(1)	3	8	1	0	0	1	No	80/5/02 00
39	80/5/02(2)	0	0	0	0	0	0	No	N/A
40	80/5/15	0	0	0	0	1	0	Yes	B
41	80/5/16	0	0	0	0	1	0	Yes	B
42	80/5/18	0	10	2	0	0	0	No	80/5/18 00
43	80/5/27	0	3	1	0	1	1	No	B
44	80/5/29(1)	2	0	3	0	2	0	Yes	80/5/29 00
45	80/5/29(2)	0	0	0	0	0	0	No	80/5/29 12
46	80/5/30	5	8	2	0	2	0	Yes	N/A
47	80/6/17	3	3	1	2	7	0	No	80/6/17 00
48	80/6/19	1	5	7	0	5	0	Yes	80/6/19 00
49	80/6/20(1)	0	2	1	0	0	0	Yes	N/A
50	80/6/20(2)	0	1	1	0	2	0	Yes	80/6/20 00
51	80/6/20(3)	0	0	5	0	0	0	Yes	N/A
52	80/6/20(4)	0	1	1	0	0	0	Yes	N/A
53	81/5/09(1)	0	2	0	0	0	0	No	81/5/08 12
54	81/5/09(2)	0	0	0	0	0	0	No	81/5/09 00
55	81/5/24	2	4	3	0	0	0	No	81/5/24 00
56	81/5/29(1)	1	2	2	0	0	2	Yes	81/5/28 12
57	81/5/29(2)	1	0	2	0	0	0	Yes	81/5/29 00
58	81/5/30	0	0	0	0	0	0	No	81/5/30 00
59	81/6/02	4	9	0	1	3	0	No	81/6/02 00
60	81/6/03	0	3	2	1	0	0	No	81/6/03 00
61	81/6/15	0	0	1	0	1	0	No	81/6/15 00
62	81/6/16	0	0	0	1	1	0	No	B
63	82/5/06	0	1	0	0	4	0	No	82/5/06 00
64	82/5/12	1	7	0	0	4	0	Yes	82/5/12 00
65	82/5/16	2	3	0	0	4	2	Yes	82/5/16 00
66	82/5/17	8	5	2	1	20	0	Yes	82/5/17 00
67	82/5/24(1)	0	0	0	0	0	0	No	82/5/23 12
68	82/5/24(2)	0	0	0	1	0	0	No	82/5/24 00
69	82/5/28	3	0	13	3	0	0	No	82/5/28 00
70	82/6/16	0	2	3	0	1	0	Yes	82/6/16 00
71	82/6/24(1)	0	5	5	1	0	0	No	82/6/23 12
72	82/6/24(2)	0	0	0	0	2	0	No	82/6/24 00

in columns B–K of given row of the matrix; the resulting value of C is entered in column L.

Values of C may (at least theoretically) range from −10 to 10 in increments of 0.5 (although in practice, values less than −5 were rarely tallied). Since columns B–K contain the basic ten characteristics of ll/ts structure enumerated in section 4, C = 10 indicates the maximum possible degree of leading-line/trailing-stratiform structure that can be shown by our system of evaluation. To determine whether the structure of a particular MPS more closely resembled the Symmetric Case or the Asymmetric Case, we further computed the quantity

S = Sum of the numbers recorded in columns M and N, entered in column O.

Values of S range from −2 to 2, also in increments of 0.5. Positive values of S indicate similarity to the Symmetric case, while negative values indicate similarity to the Asymmetric Case.

Acknowledgments. The radar microfilms for this study were made available by the National Severe Storms Laboratory (NSSL). Satellite data were provided by Professor A. H. Thompson of Texas A&M University, and Dr. E. Tollerud and Mr. Dennis Rodgers of the NOAA/ERL Forecast Systems Laboratory (FSL). Shao-wen Shou and David Kingsmill assisted with early versions of the satellite and sounding data analyses. Terri Rottman and Abhik Biswas assisted with much of the data reduction. Barry Schwartz (FSL) and David Blanchard (NSSL) provided sounding data and analysis software, respectively. Figures were drafted with the assistance of Kay Dewar and Jim Adams. Comments by Drs. M. Weisman and M. LeMone and an anonymous reviewer greatly improved the manuscript. Candace Gudmundson edited the manuscript. This research was supported by the National Science Foundation under Grant ATM-8719838 and by the National Severe Storms Laboratory under Grant NA80RAD00025.

REFERENCES

Balaji, V., and T. L. Clark, 1988: Scale selection in locally forced convective fields and the initiation of deep cumulus. *J. Atmos. Sci.*, **45**, 3188–3211.

Bartels, D. L., J. M. Skradski and R. D. Menard, 1984: Mesoscale convective systems: A satellite-data-based climatology. NOAA Tech Mem., ERL-ESG-8, 58 pp. [Available from National Severe Storms Lab. Mesoscale Research Div., 325 Broadway, Boulder, CO 80207.]

Bluestein, H. B., and M. H. Jain, 1985: Formation of mesoscale lines of precipitation: Severe squall lines in Oklahoma during the spring. *J. Atmos. Sci.*, **42**, 1711–1732.

——, G. T. Marx and M. H. Jain, 1987: Formation of mesoscale lines of precipitation: Non-severe squall lines in Oklahoma during the spring. *Mon. Wea. Rev.*, **115**, 2719–2727.

Bonner, W. D., 1968: Climatology for the low level jet. *Mon. Wea. Rev.*, **96**, 833–850.

Chappell, C. F., 1986: Quasi-stationary convective events. *Mesoscale Meteorology and Forecasting*, P. S. Ray, Ed., American Meteorological Society, Boston, 289–310.

Cheng, C.-P., and R. A. Houze, Jr., 1979: The distribution of convective and mesoscale precipitation in GATE radar-echo patterns. *Mon. Wea. Rev.*, **107**, 1370–1381.

Chong, M., P. Amayenc, G. Scialom and J. Testud, 1987: A tropical squall line observed during the COPT'81 experiment in West Africa. Part I: Kinematic structure inferred from dual-Doppler radar data. *Mon. Wea. Rev.*, **115**, 670–694.

Churchill, D. D., and R. A. Houze, Jr., 1984: Development and structure of winter monsoon cloud clusters on 10 December, 1978. *J. Atmos. Sci.*, **41**, 933–960.

Davies-Jones, R. P., 1984: Streamwise vorticity: The origin of updraft rotation in supercell storms. *J. Atmos. Sci.*, **41**, 2991–3006.

Dodge, P., 1985: Mesoscale rain events in the spring over Oklahoma. M.S. thesis, University of Washington, 167 pp. [Available from Dept. of Atmospheric Sciences AK-40, University of Washington, Seattle, WA 98195.]

Fawbush, E. J., and R. C. Miller, 1954: The types of air masses in which North American tornadoes form. *Bull. Amer. Meteor. Soc.*, **35**, 154–165.

Fortune, M., 1980: Properties of African disturbance lines inferred from time-lapse satellite imagery. *Mon. Wea. Rev.*, **108**, 153–168.

Foster, D. S., 1958: Thunderstorm gusts compared with computed downdraft speeds. *Mon. Wea. Rev.*, **86**, 91–94.

Fovell, R. G., and Y. Ogura, 1988: Numerical simulation of a midlatitude squall line in two dimensions. *J. Atmos. Sci.*, **45**, 3846–3879.

——, and ——, 1989: Effect of vertical wind shear on numerically simulated multicell storm structure. *J. Atmos. Sci.*, **46**, 3144–3176.

Fritsch, J. M., R. J. Kane and C. R. Chelius, 1986: The contribution of mesoscale convective weather systems to the warm-season precipitation in the United States. *J. Climate Appl. Meteor.*, **25**, 1333–1345.

Fujita, T. T., 1955: Results of detailed synoptic studies of squall lines. *Tellus*, **7**, 405–436.

——, 1959: Precipitation and cold air production in mesoscale thunderstorm systems. *J. Meteor.*, **16**, 454–466.

——, 1981: Tornadoes and downbursts in the context of generalized planetary scales. *J. Atmos. Sci.*, **38**, 1511–1534.

Gamache, J. F., and R. A. Houze, Jr., 1982: Mesoscale air motions associated with a tropical squall line. *Mon. Wea. Rev.*, **110**, 118–135.

——, and ——, 1983: Water budget of a mesoscale convective system in the tropics. *J. Atmos. Sci.*, **40**, 1835–1850.

——, and ——, 1985: Further analysis of the composite wind and thermodynamic structure of the 12 September GATE squall line. *Mon. Wea. Rev.*, **113**, 1241–1259.

Hauf, T., and T. L. Clark, 1989: Three-dimensional numerical experiments on convectively forced internal gravity waves. *Quart. J. Roy. Meteor. Soc.*, **115**, 309–333.

Heymsfield, G. M., and S. Schotz, 1985: Structure and evolution of a severe squall line over Oklahoma. *Mon. Wea. Rev.*, **113**, 1563–1589.

Houze, R. A., Jr., 1973: A climatological study of vertical transports by cumulus-scale convection. *J. Atmos. Sci.*, **30**, 1112–1123.

——, 1977: Structure and dynamics of a tropical squall-line system. *Mon. Wea. Rev.*, **105**, 1540–1567.

——, and A. K. Betts, 1981: Convection in GATE. *Reviews of Geophysics and Space Physics*, **19**, 541–576.

——, and E. N. Rappaport, 1984: Air motions and precipitation structure of an early summer squall line over the eastern tropical Atlantic. *J. Atmos. Sci.*, **41**, 553–574.

——, S. A. Rutledge, M. I. Biggerstaff and B. F. Smull, 1989: Interpretation of Doppler weather radar displays of midlatitude mesoscale convective systems. *Bull. Amer. Meteor. Soc.*, **70**, 608–619.

Johns, R. H., and W. D. Hirt, 1987: Derechos: Widespread convectively induced windstorms. *Wea. Forecasting*, **2**, 32–49.

Kelly, D. L., J. T. Schaefer, R. P. McNulty, C. A. Doswell III and

R. F. Abbey, Jr., 1978: An augmented tornado climatology. *Mon. Wea. Rev.*, **106,** 1172–1183.

Kessinger, C. J., P. S. Ray and C. E. Hane, 1987: The Oklahoma squall line of 19 May 1977. Part I: A multiple-Doppler analysis of convective and stratiform structure. *J. Atmos. Sci.*, **44,** 2840–2864.

Leary, C. A., and E. N. Rappaport, 1987: The life cycle and internal structure of a mesoscale convective complex. *Mon. Wea. Rev.*, **115,** 1503–1527.

Lilly, D. K., 1983: Dynamics of rotating thunderstorms. *Mesoscale Meteorology—Theories, Observations, and Models,* D. K. Lilly and T. Gal-Chen, Eds., Reidel, 531–544.

Maddox, R. A., 1980: Mesoscale convective complexes. *Bull. Amer. Meteor. Soc.*, **61,** 1374–1387.

——, D. M. Rodgers and K. W. Howard, 1982: Mesoscale convective complexes over the United States during 1981—Annual summary. *Mon Wea. Rev.*, **110,** 1501–1514.

Newton, C. W., 1950: Structure and mechanisms of the prefrontal squall line. *J. Meteor.*, **7,** 210–222.

——, and J. C. Fankhauser, 1964: On the movements of convective storms, with emphasis on size discrimination in relation to water-budget requirements. *J. Appl. Meteor.*, **3,** 651–668.

Ogura, Y., and M.-T. Liou, 1980: The structure of a midlatitude squall line. *J. Atmos. Sci.*, **37,** 553–567.

Pedgley, D. E., 1962: A meso-synoptic analysis of the thunderstorms on 28 August, 1958. *Brit. Meteor. Off., Geophys. Mem.*, No. 106, 74 pp.

Rodgers, D. M., K. W. Howard and E. C. Johnston, 1983: Annual summary—Mesoscale convective complexes over the United States during 1982. *Mon. Wea. Rev.*, **111,** 2363–2369.

Rotunno, R., J. B. Klemp and M. L. Weisman, 1988: A theory for strong, long-lived squall lines. *J. Atmos. Sci.*, **45,** 463–485.

Roux, F., J. Testud, M. Payen and B. Pinty, 1984: West African squall-line thermodynamic structure retrieved from dual-Doppler radar observations. *J. Atmos. Sci.*, **41,** 3104–3121.

Rutledge, S. A., and D. R. MacGorman, 1988: Cloud-to-ground lightning activity in the 10–11 June 1985 mesoscale convective system observed during the Oklahoma-Kansas PRE-STORM project. *Mon. Wea. Rev.*, **116,** 1393–1408.

——, R. A. Houze, Jr., M. I. Biggerstaff and T. Matejka, 1988: The Oklahoma-Kansas mesoscale convective system of 10–11 June 1985: Precipitation structure and single-Doppler radar analysis. *Mon. Wea. Rev.*, **116,** 1409–1430.

Smull, B. F., and R. A. Houze, Jr., 1985: A midlatitude squall line with a trailing region of stratiform rain: Radar and satellite observations. *Mon. Wea. Rev.*, **113,** 117–133.

——, and ——, 1987a: Dual-Doppler radar analysis of a midlatitude squall line with a trailing region of stratiform rain. *J. Atmos. Sci.*, **44,** 2128–2148.

——, and ——, 1987b: Rear inflow in squall lines with trailing-stratiform precipitation. *Mon. Wea. Rev.*, **115,** 2869–2889.

Srivastava, R. C., T. J. Matejka and T. J. Lorello, 1986: Doppler radar study of the trailing anvil region associated with a squall line. *J. Atmos. Sci.*, **43,** 356–377.

Watson, A. I., J. G. Meitin and J. B. Cunning, 1988: Evolution of the kinematic structure and precipitation characteristics of a mesoscale convective system on 20 May 1979. *Mon. Wea. Rev.*, **116,** 1555–1567.

Weisman, M. L., and J. B. Klemp, 1982: The dependence of numerically simulated convective storms on wind shear and buoyancy. *Mon. Wea. Rev.*, **110,** 504–520.

——, —— and R. Rotunno, 1988: Structure and evolution of numerically simulated squall lines. *J. Atmos. Sci.*, **45,** 1990–2013.

Zipser, E. J., 1969: The role of organized unsaturated convective downdrafts in the structure and rapid decay of an equatorial disturbance. *J. Appl. Meteor.*, **8,** 799–814.

——, 1977: Mesoscale and convective-scale downdrafts as distinct components of squall-line circulation. *Mon. Wea. Rev.*, **105,** 1568–1589.

——, 1983: Use of a conceptual model of the life cycle of mesoscale convective systems to improve very short-range forecasts. *Nowcasting,* K. Browning, Ed. 191–204.